

## EXAMINING STRUCTURAL AND RELATED SPECTRAL CHANGE IN MARS-RELEVANT PHYLLOSILICATES AFTER EXPERIMENTAL IMPACTS BETWEEN 10–40 GPa

LONIA R. FRIEDLANDER<sup>1,\*</sup>, TIMOTHY D. GLOTCH<sup>1</sup>, BRIAN L. PHILLIPS<sup>1</sup>, JOHN S. VAUGHN<sup>1</sup>, AND JOSEPH R. MICHALSKI<sup>2</sup>

<sup>1</sup> Geosciences Department, 255 Earth and Space Sciences (ESS) Building, Stony Brook University, Stony Brook, NY, 11794-2100 USA

<sup>2</sup> Planetary Science Institute, 1700 E. Fort Lowell, Tucson, AZ, 85719 USA

**Abstract**—Accurate clay mineral identification is key to understanding past aqueous activity on Mars, but martian phyllosilicates are old (>3.5 Ga) and have been heavily bombarded by meteoroid impacts. Meteoroid impacts can alter clay mineral structures and spectral signatures, making accurate remote sensing identifications challenging. This paper uses nuclear magnetic resonance (NMR) spectroscopy to examine the short-range structural deformation induced in clay mineral samples of known composition by artificial impacts and calcination. Structural changes are then related to changes in the visible-near infrared (VNIR) and mid-infrared (MIR) spectra of these clay mineral samples. The susceptibility of phyllosilicates to structural deformation after experimental impacts varies by structure. Experimental results showed that trioctahedral, Mg(II)-rich saponite was structurally resilient up to peak pressures of 39.8 GPa and its unchanged post-impact spectra reflected this. Experimental data on kaolinite showed that this Al(III)-rich, dioctahedral phyllosilicate was susceptible to structural alteration at peak pressures  $\geq 25.1$  GPa. This result is similar to previously reported experimental results on the Fe(III)-rich dioctahedral smectite nontronite, suggesting that dioctahedral phyllosilicates may be more susceptible to shock-induced structural deformation than trioctahedral phyllosilicates. The octahedral vacancies present in dioctahedral phyllosilicates may drive this increased susceptibility to deformation relative to trioctahedral phyllosilicates with fully occupied octahedral sheets. Thermal alteration accompanies shock in meteoroid impacts, but shock differs from thermal alteration. NMR spectroscopy showed that structural deformation in thermally altered phyllosilicates differs from that found in shocked phyllosilicates. Similar to shock, dioctahedral phyllosilicates are also more susceptible to thermal alteration. This differential susceptibility to impact-alteration may help explain generic smectite identifications from heavily bombarded terrains on Mars.

**Key Words**—Dioctahedral Phyllosilicates, Martian Remote Sensing, Meteoroid Impacts, Structural Deformation, Trioctahedral Phyllosilicates.

### INTRODUCTION

Extensive clay mineral deposits have been identified on Mars by orbital VNIR reflectance spectroscopic remote sensing techniques (Poulet *et al.*, 2005, 2009; Clark *et al.*, 2007; Loizeau *et al.*, 2007; Mustard *et al.*, 2008; McKeown *et al.*, 2009; Wray *et al.*, 2009; Fairén *et al.*, 2010; Michalski *et al.*, 2010; Ehlmann *et al.*, 2011; Che and Glotch, 2014). The identification of phyllosilicates on Mars is exciting because phyllosilicates provide evidence for past aqueous environments on the martian surface, which are associated with past and current potential habitability (Michalski and Noe Dobrea, 2007; Poulet *et al.*, 2009; Grotzinger *et al.*, 2014). To fully understand these ancient environments, identification of the clay minerals observed on the martian surface must be as specific as possible. Clay minerals on Mars, however, are often found in ancient

environments that have experienced extensive meteoroid bombardment. Bibring *et al.* (2006) noted that both in Syrtis Major and Nili Fossae, for example, phyllosilicate-rich rocks are detected within ancient craters, as well as ancient terrains recently excavated by meteoroid impacts. The association of martian phyllosilicates with impacts may complicate identification by remote sensing because impact-induced alteration can alter mineral spectral signatures (Tarte *et al.*, 1990).

Despite these challenges, certain specific phyllosilicates have been either identified or are hypothesized in multiple locations on Mars. Martian clay mineral deposits are thought to be dominantly smectitic on the basis that many of the infrared detections of phyllosilicates on Mars exhibit absorptions near 1.9  $\mu\text{m}$  ( $5263\text{ cm}^{-1}$ ), corresponding to adsorbed and interlayer  $\text{H}_2\text{O}$ , as well as  $\text{M}_x\text{OH}$  bending bands at  $\sim 2.2\text{--}2.3\text{ }\mu\text{m}$  ( $4545\text{--}4348\text{ cm}^{-1}$ ). One of the most commonly identified phases is an iron-rich smectite similar to nontronite, but ambiguous Fe/Mg-rich smectite identifications are also common (Carter *et al.*, 2013). The presence of nontronite has been hypothesized at many

\* E-mail address of corresponding author:

loniarf@gmail.com

DOI:10.1346/CCMN.2016.0640302

locations in the southern highlands of Mars, but the least ambiguous detections have been concentrated in Nili Fossae (Bibring *et al.*, 2005; Poulet *et al.*, 2005; Che and Glotch, 2014), Mawrth Vallis (Loizeau *et al.*, 2007), and Syrtis Major (Bibring *et al.*, 2006). In these regions, phyllosilicate identification frequently coincides with evidence of meteoroid impacts (*e.g.* Bibring *et al.*, 2006). Nontronite has also been proposed as a best-match for reflectance spectra detected by the Compact Reconnaissance Imaging Spectrometer for Mars (CRISM) from Cape York at Endeavor Crater, a 22-km impact crater in Meridiani Planum (Arvidson *et al.*, 2014). Mg(II)-rich saponite has been unambiguously detected in northern Sinus Meridiani (Wiseman *et al.*, 2010). *In-situ* X-ray diffraction (XRD) of sedimentary rocks from Yellowknife Bay in Gale Crater has also revealed the presence of trioctahedral smectites, likely saponite or Fe-saponite, although it is as yet unclear why these smectites have expanded structures with 02l peaks observed at higher 2 $\theta$  than terrestrial saponite (Vaniman *et al.*, 2014). Additional results from the Sample Analysis at Mars (SAM) instrument at the same location were consistent with both di- and trioctahedral smectites, including nontronite (Archer *et al.*, 2014). Perhaps the identification of the trioctahedral smectites at Gale Crater by XRD is complicated by impact-alteration and the presence of a partially amorphous dioctahedral smectite, such as impact-altered nontronite (*e.g.* Friedlander *et al.*, 2015). Finally, the 1:1 dioctahedral clay mineral, kaolinite, has been unambiguously identified in several regions of Mars, including Valles Marineris and Terra Meridiani, where it partially infills highland craters in layered deposits together with hydrated sulfates (Murchie *et al.*, 2009; Wray *et al.*, 2009).

The coincidence of martian clay mineral detections with the evidence of meteoroid impacts implies that martian phyllosilicates are old. The older the martian phyllosilicates are, the more impacts are likely to have strongly affected their geochemical history (Hartmann, 1966; Hartmann and Neukum, 2001). This reasoning is self-consistent; thus, the secondary confirmation of the relative ages of martian phyllosilicate deposits by studies of martian geomorphology is helpful. Martian geomorphology studies often show that phyllosilicate-bearing units underlie (and, therefore, pre-date) other hydrated mineral deposits. Hydrated minerals are thought to have formed in an early epoch of martian geologic history during which the surface of Mars is hypothesized to have been significantly wetter than it is today (Ehlmann *et al.*, 2009; Murchie *et al.*, 2009; Mustard *et al.*, 2009; Wray *et al.*, 2009; Wiseman *et al.*, 2010). As a result, martian phyllosilicates are widely considered to be ancient and likely experienced extensive alteration by meteoroid bombardment.

Despite observations of their relatively old age, planetary scientists have not wholly established whether

all martian phyllosilicates necessarily pre-date meteoroid bombardment. In particular, the questions of whether phyllosilicates detected within impact craters pre- or post-date (Fairén *et al.*, 2010; Marzo *et al.*, 2010) the craters themselves or form as a result of impact-driven or post-impact alteration are still unresolved (Mangold *et al.*, 2007; Poulet *et al.*, 2008; Mustard *et al.*, 2009; Fairén *et al.*, 2010; Furukawa *et al.*, 2011; Ehlmann *et al.*, 2013; Tornabene *et al.*, 2013). At the scale of the planetary surface, however, phyllosilicates are commonly found in heavily bombarded terrains on Mars (Carter *et al.*, 2013), and such terrains are thought to be ancient (Hartmann, 1966; Tanaka, 1986, 2005); thus, any phyllosilicates that did pre-date bombardment likely experienced impact-driven alteration.

One line of evidence for martian phyllosilicates pre-dating at least some impact craters comes from the martian meteorites. Including the long-known SNC meteorites, where SNC stands for the three meteorite types (Shergottites, Nakhilites, and Chassignites) that were originally recognized as significantly different from most other meteorites, the martian meteorites are thought to have been launched to Earth by meteoroid impacts on the martian surface and may, therefore, reflect the composition of the martian surface at the time of these impacts (McSween, 1994; Hamilton *et al.*, 2003). Many detections of phyllosilicates have been made in the martian meteorites (Treiman *et al.*, 1993; Brearley, 2000; Thomas-Keprta *et al.*, 2000). The clay minerals identified in martian meteorites occur as vein-filling, crosscutting veinlets, and intergranular alteration films (Gooding *et al.*, 1990, 1991; Treiman *et al.*, 1993; Thomas-Keprta *et al.*, 2000). The complex relationship of these clay minerals to the other grains in the martian meteorites implies formation prior to the samples' launch by meteoroid impacts (McSween, 1994). The presence of clay minerals in martian meteorites prior to launch and arrival on Earth implies that Mars (at some point early in its geologic history) supported the formation of hydrated alteration products at or near its surface. Their detection in meteorite samples also implies that these clay minerals can survive impacts, although the extent and pathway of possible alteration by impact exposure is difficult to quantify for such clays. Unfortunately, the complex geochemistry and the limited number and size (available mass) of martian meteorite samples makes it impractical to conduct destructive experiments, such as impact experiments, on them. In the present study, the impact experiments were conducted on The Clay Minerals Society (CMS) Source Clays Repository samples of known composition. Impact experiments were intended to simulate meteoroid impacts, reproducing the extreme pressure and temperature conditions to which target material is subjected during impacts.

During meteoroid impacts, intense pressure and heat waves are generated. This distinct wave of extreme  $P$ ,  $T$

conditions is known as a shock wave (Langenhorst, 2002). Shock waves differ from other pressure waves, such as seismic (elastic) waves, by their very short durations and sharply discontinuous initial stress curves. Shock waves produce unique stress curves as a result of the very short timescales in which they pass through the material, on the order of 1 s for the natural impact of a 10 km diameter projectile. Shock waves initiate geologically distinct processes that cause structural alteration as the minerals in the target material adapt to extreme  $P$ ,  $T$  conditions with strain rates on the order of  $10^6$ – $10^9$  s $^{-1}$  (French, 1998). Existing defects may be propagated, high-pressure polymorphs are activated from liquidus phase structures, and structural disorder increases (Gault and Heitowitz, 1963; Stöffler, 1972, 1974, 1984; Hanss *et al.*, 1978; Lange and Ahrens, 1982; Bischoff and Stöffler, 1992; Langenhorst, 2002).

Shock effects are also unique because  $P$  and  $T$  drop off sharply in a steep gradient with distance from the impact point. Peak shock pressure decreases exponentially and temperature depends on the shock pressure experienced by target material along with the density and compressibility of the minerals present (French, 1998). At the furthest distances from the impact point, shock waves become normal elastic waves and do not produce any permanent deformation of the kind observed for shocked material (French, 1998). The entire transit of the shock wave is during the contact stage of an impact, which lasts no more than a few seconds and, for most impacts, is over in fractions of a second (French, 1998). Shock also induces high temperatures in target materials. Melting is rare, but it does occur (*e.g.* Stöffler, 1984). Impacts with shock pressures of up to 45 GPa, higher than the highest impact pressures discussed here, produce post-shock temperatures on the order of 300–900°C, low enough that nearly no actual melting occurs. In contrast to the nearly instantaneous passing of the initial shockwave, however, elevated post-shock temperatures can persist in target rock assemblies for as long as hours to days, and possibly years as indicated by some modeling results. These elevated temperatures still drop off steeply from the impact point, however, making the shock effects of both  $P$  and  $T$  local and dependent on crater size and distance from the impact point (Bogard and Hirsch, 1980; Abramov and Kring, 2005).

To measure the effects of impacts on mineral structures and spectroscopic signatures, laboratory impact experiments can be used to generate controlled, experimental impacts. Because the impact conditions are precisely known, impact experiments allow structural and spectral changes in shocked minerals to be associated with known velocities and calculated peak pressures or pressure ranges (De Carli and Jamieson, 1959; Gibbons and Ahrens, 1971; Stöffler, 1972, 1974, 1984; Hanss *et al.*, 1978; Adams *et al.*, 1979; Johnson *et*

*al.*, 2002, 2007; Johnson and Hörz, 2003). Such experiments also provide libraries of impact-altered spectral end-member data, which are useful for remote sensing image analysis (*e.g.* Bibring *et al.*, 2005; Poulet *et al.*, 2005; Bishop *et al.*, 2008a; Mustard *et al.*, 2008; Arvidson *et al.*, 2014).

Laboratory impact experiments go back to the first recognition of shock as a fundamental geologic process (Stöffler, 1972, 1974; Bischoff and Stöffler, 1992). The marriage of laboratory impacts with infrared spectroscopy has been especially fruitful. Distinct changes in the reflectance spectra of shocked *versus* unshocked plagioclase, pyroxene, and glass have been revealed (Adams *et al.*, 1979; Johnson and Hörz, 2003). The spectral effects of laboratory impacts on pyroxene have been shown to differ from those on feldspar (Johnson *et al.*, 2002). Natural basalt samples, both in independent experiments (Johnson *et al.*, 2007) and in comparison experiments with collected samples from impact structures on Earth (Kieffer *et al.*, 1976), have been exposed to laboratory impacts. Phyllosilicates, however, are largely absent from this large body of work. This may be partially due to the early belief that layered silicates were largely stable after impacts. Investigations of natural samples from terrestrial impact structures demonstrated that layered silicates showed remarkable stability, relative to other minerals, even at shock pressures exceeding 300 kbar (30 GPa). Hörz and Ahrens (1969) investigated kinked micas in impact-altered samples and showed that, despite large-scale physical deformation, their mica samples remained unchanged at the sub-unit cell scale. Later work did show, however, that shocked phyllosilicates dehydrated faster than unshocked samples (Boslough *et al.*, 1980; Lange and Ahrens, 1982; Tyburczy and Ahrens, 1987). Nonetheless, the possibility that exposure to impacts would induce structural deformation in phyllosilicates was not initially clear.

Early evidence in favor of observable impact alteration effects in phyllosilicate spectroscopy came from Weldon *et al.* (1982). Using various spectroscopic techniques, they determined that partial dehydroxylation changed the Fe-coordination state of a Riverside nontronite sample after experimental impacts between 180–300 kbar (18–30 GPa). As a result, the Fe $^{3+}$ /O $^{2-}$  charge transfer absorption edge shifted from the ultraviolet into the visible wavelength region, producing a redder, darker nontronite sample. Weldon *et al.* (1982) suggested that these post-impact changes might explain the color of the martian surface, but they also attributed their results primarily to impact-induced heating. Later work showed, however, that the effects of shock differed from those of heat. Results from X-ray diffraction (XRD) comparisons showed that post-shock samples of Riverside nontronite were structurally distinct from heated samples (Boslough *et al.*, 1986). More recent work showed that experimental impacts induced struc-

tural degradation and partial amorphization in several dioctahedral phyllosilicates (*e.g.* Gavin *et al.*, 2013). Structural alteration was detected in the XRD patterns and MIR reflectance spectra of post-impact samples, while their near-infrared (NIR) spectra remained largely unchanged. The authors hypothesized that this might be due to the relatively low (<200°C) peak temperatures achieved in many of their experiments and the fact that structural degradation occurred without irreversible dehydration/dehydroxylation. The highest peak pressure reported by Gavin *et al.* (2013), however, was only 17.5 GPa. This may be another reason why they reported unchanged NIR reflectance spectra. In contrast, data from experimental impacts on nontronite at higher peak pressures showed that nontronite's VNIR reflectance spectrum does change at high peak pressures (*e.g.* Friedlander *et al.*, 2015).

The objective of the present study was to provide data on the effects of shock on two Mars-relevant phyllosilicates, a trioctahedral smectite (saponite), and a dioctahedral 1:1 phyllosilicate (kaolinite), and to compare these results to previously published results on nontronite. The comparison between trioctahedral and dioctahedral phyllosilicates is particularly useful for understanding how impact effects differ by structure among phyllosilicates. Using the best available experimental impact techniques, shock effects were explored largely independent of thermal alteration. The use of NMR spectroscopy as an analysis technique also helped to clarify how impacts affect cation-bonding environments in phyllosilicates and, especially, how thermal alteration differs from shock. The spectroscopic results described below also revealed structural alteration trends in shocked phyllosilicates that may be useful for interpreting remote sensing data from Mars.

## MATERIALS AND METHODS

All phyllosilicate samples used in these experiments are from the CMS Source Clays Repository: saponite (SapCa-2) and kaolinite (KGa-1b). The compositions, structures, and IR spectra of these phases have been well characterized (Post, 1984; Madejová and Komadel, 2001; Mermut and Cano, 2001; Moll, 2001).

### Sample preparation

To remove any impurities occurring in the >2  $\mu\text{m}$  size fraction (Moore and Reynolds, 1989), all phyllosilicate samples were ground, sieved, and the <2  $\mu\text{m}$  size fraction separated for use in the impact experiments and subsequent analysis. The >2  $\mu\text{m}$  size fraction was not used. The grain-size separation methods used have been described previously in detail for nontronite (Friedlander *et al.*, 2015) and are based on the method introduced by Moore and Reynolds (1989). In a final purification step, separated clay mineral samples were washed with acetic acid to remove carbonate impurities.

### Impact experiments

Impact experiments were performed at the Flat Plate Accelerator (FPA) at NASA's (National Aeronautics and Space Administration) Johnson Space Center (JSC). Peak shock pressures produced by the FPA are derived using the measured projectile velocity and the shock impedances of the flyer plate and sample assembly via the Rankine-Hugoniot equations (Rankine, 1870; Hugoniot, 1889; Gault and Heitowit, 1963) and are achieved *via* shock-reverberation. Peak shock pressures achieved by shock-reverberation differ in both strain-rate and pathway from the Hugoniot for naturally shocked samples (*e.g.* Stöffler, 1972, 1974; Stöffler and Langenhorst, 1994; Grieve *et al.*, 1996). The largest material response difference caused by the different strain rates and pathways of shock reverberation and natural shock is in the thermal state of the material (Gibbons and Ahrens, 1971). The lesser amount of work done in a shock-reverberation experiment to compress the sample to peak pressure, as compared to a natural shock event, means that the temperature will be significantly lower during the shock-reverberation experiment (Kraus *et al.*, 2013 and additional citations therein). The differences between shock-reverberation and natural impacts make shock-reverberation and recovery experiments the best method available to investigate shock, independent from thermal alteration effects in mineral samples.

Pore space in experimental shock-recovery methods is of great concern. For the experiments performed, sample powders were pressed into pellets (to minimize pore space) and loaded into stainless steel sample containers that were individually milled to match the dimensions of each pellet. Pressed pellets reduce the initial porosity of the sample and the entropy added to the system by potential pore collapse (Kieffer, 1971). On average, each shock experiment used 0.15 g of sample. Stainless steel and fansteel flyer plates were used to produce impacts approximating one-dimensional shock (See *et al.*, 2012). Projectiles were launched horizontally at the mounted, vertically oriented sample containers and their velocities were measured directly by lasers in the flight path. These velocities were converted to pressure by one-dimensional shock-stress calculations after Gault and Heitowit (1963), giving shock-stress accuracies of  $\pm 1\%$ . The experiments covered peak pressures ranging from 10–20 GPa in a single 10 GPa step and 25–40 GPa in 5 GPa increments. Peak pressures varied by sample and experimental run (Table 1). The tilt of the projectile must be less than  $3^\circ$  to approximate one-dimensional shock. Dual cameras stationed along the flight path monitored the projectile tilt. Samples from impacts with tilts greater than  $3^\circ$  were not used in this study. After successful experiments, sample containers were milled open, enabling recovery of nearly the entire  $\sim 0.15$  g shocked sample. Samples

Table 1. Target and flyer plate assembly materials, measured impactor velocities (km/s), and calculated shock pressures (GPa) for all of the impact shock experiments conducted on the clay mineral samples described in this manuscript.

Clay Sample	Target assembly material	Flyer plate material	Impactor velocity (km/s)	Calculated pressure (GPa)
Saponite	Stainless steel	Aluminum	0.870	10.2
	Stainless steel	Stainless steel	0.986	20.6
	Stainless steel	Stainless steel	1.156	24.9
	Stainless steel	Stainless steel	1.331	29.4
	Fansteel	Stainless steel	1.299	35.0
	Fansteel	Stainless steel	1.369	39.8
Kaolinite	Stainless steel	Aluminum	0.871	10.2
	Stainless steel	Stainless steel	0.947	19.7
	Stainless steel	Stainless steel	1.164	25.1
	Stainless steel	Stainless steel	1.339	29.3
	Fansteel	Stainless steel	1.251	35.6
	Fansteel	Stainless steel	1.361	39.6

were stored in unsealed plastic containers and equilibrated to ambient temperature and humidity conditions before shipping to the Vibrational Spectroscopy Laboratory at Stony Brook University. Once there, the samples were stored in sealable plastic tubes in a cabinet desiccator in the presence of Drierite<sup>™</sup> desiccant (W.A. Hammond DRIERITE Co. Ltd., Xenia, Ohio, U.S.A.) both prior to and after measurement by vibrational spectroscopy techniques.

#### Visible-near infrared and mid-infrared spectroscopic methods

VNIR reflectance, MIR emissivity, and MIR attenuated total reflectance (ATR) spectra were acquired at the Vibrational Spectroscopy Laboratory at Stony Brook University. VNIR bidirectional reflectance spectra of each sample were collected between 0.35–2.5  $\mu\text{m}$  (28571–4000  $\text{cm}^{-1}$ ) on an ASD Instruments (now PANalytical, Boulder, Colorado, U.S.A.) Field Spec 3 Max Spectroradiometer fitted with an 8-degree field of view foreoptic. This instrument uses three detectors to cover the relevant VNIR wavelength range: a VNIR 512-element silicon diode array for the 0.35–1.00  $\mu\text{m}$  wavelength region (28571–10000  $\text{cm}^{-1}$ ), one shortwave infrared (SWIR) camera with a thermoelectrically (TE) cooled InGaAs photodiode for the 1.00–1.83  $\mu\text{m}$  wavelength region (10000–5464  $\text{cm}^{-1}$ ), and a second SWIR camera with another TE-cooled InGaAs photodiode for the 1.83–2.50  $\mu\text{m}$  wavelength region (5464–4000  $\text{cm}^{-1}$ ). As a result, the spectral resolution of the instrument varies by wavelength region. At 0.70  $\mu\text{m}$  the full-width-at-half-maximum (FWHM) spectral resolution is 3 nm, and it is 10 nm at both 1.40 and 2.10  $\mu\text{m}$ . For the spectral region 0.35–1.00  $\mu\text{m}$ , the instrument has a sampling interval of 1.4 nm; and for the region 1.00–2.50  $\mu\text{m}$ , it has a sampling interval of 2 nm (ASD Inc., 2010). A white-light quartz halogen lamp was used in all VNIR reflectance measurements. The

collected reflectance spectra were converted to relative reflectance by reference to an isotropic Spectralon<sup>®</sup> (Labsphere, Manchester, New Hampshire, U.S.A.) calibration target. Set incidence and emergence angles of  $30 \pm 2^\circ$  and  $0^\circ$ , respectively, were used in all measurements. Samples were held in a matte-black painted sample cup that has no reflectance features in the relevant wavelength region. The ASD Field Spec 3 produces spectra that are comparable to many orbital remote sensing reflectance measurements (Ehlmann *et al.*, 2012; Friedlander *et al.*, 2015).

Reflectance measurements were conducted under a glovebag (Sigma-Aldrich, Munich, Germany) and in the presence of Drierite<sup>™</sup> desiccant (W.A. Hammond DRIERITE Co. Ltd., Xenia, Ohio, U.S.A.) to maintain a low, stable relative humidity (RH) <15%. Continuum-removal was performed on all collected spectra using ENVI version 5.1 image analysis software (Exelis Visual Information Solutions, Boulder, Colorado, U.S.A.) for Macintosh and normalized using Davinci version 2.10 (<http://davinci.asu.edu>) remote sensing data viewing and manipulation software (Arizona State University, Tempe, Arizona, U.S.A.). These are standard techniques for comparing characteristic features in reflectance spectra (*e.g.* Clark, 1999) that also ensure that comparisons between and among different samples are consistent.

Emissivity spectra in the MIR range (2000–200  $\text{cm}^{-1}$ ) were collected on a Nicolet 6700 Fourier-transform infrared (FTIR) tabletop spectrometer (Thermo Fisher Scientific Inc., Waltham Massachusetts, U.S.A.) purged of  $\text{CO}_2$  and water vapor, by switching off the attached Global IR source and measuring the emitted radiation from the heated samples directly. Prior to heating, the samples were pressed into pellets (see Che and Glotch, 2012) to increase their emittance and reduce multiple scattering (after Michalski *et al.*, 2005, 2006; Glotch *et al.*, 2007). Heated samples were maintained at

~80°C to provide adequate emissivity signal. Previous work has shown that clay minerals do not irreversibly dehydrate until exposed to temperatures of 100°C or higher and that irreversible spectral change does not occur until well above 100°C and as high as 500°C for some phyllosilicate samples (Harris *et al.*, 1992; Fitzgerald *et al.*, 1996; Roch *et al.*, 1998; Rocha, 1999; Carroll *et al.*, 2005; Gavin and Chevrier, 2010; Che *et al.*, 2011; Che and Glotch, 2012). Permanent dehydration and layer collapse as a result of heating for the purposes of measuring emissivity were, therefore, not a concern. The collected emissivity spectra were calibrated using both warm (~70°C) and hot (~100°C) blackbody standards. A CsI beamsplitter and DLaTGS detector with a CsI window were used to acquire all emissivity spectra, which were then calibrated after Ruff *et al.* (1997).

MIR ATR spectra (4000–500 cm<sup>-1</sup>) were collected on a Nicolet 6700 FTIR spectrometer (Thermo Fisher Scientific Inc., Waltham Massachusetts, U.S.A.) purged of CO<sub>2</sub> and water vapor and equipped with a Smart Orbit single-bounce ATR accessory with a type-IIA diamond ATR element. MIR ATR spectra have high spectral contrast, resembling absorption spectra acquired using standard KBr pellet preparation techniques, which they also approximate for quantitative purposes (Fahrenfort, 1961).

#### *NMR spectroscopic methods*

NMR spectroscopic data were collected at Stony Brook University. Data for both <sup>29</sup>Si and <sup>27</sup>Al were collected for all possible clay mineral samples (excluding iron-rich samples, such as nontronite) and <sup>23</sup>Na for the shocked saponite. The single-pulse magic angle spinning (SP/MAS) spectra were collected for <sup>29</sup>Si with a 400 MHz (9.4 tesla - T) Varian Inova spectrometer (Varian, Inc., Palo Alto, California, U.S.A.) operating at 79.5 MHz, using Varian/Chemagnetics T3 sample probe assemblies (Varian, Inc., Palo Alto, California, U.S.A.) configured for either 7.5 mm or 3.2 mm (outside diameter - o.d.) rotors. Spectra for the heat-treated kaolinite samples were acquired with the 7.5 mm probe assembly using 8 μs (90°) pulses with 2 s relaxation delays at a spinning rate of 5 kHz. Additional data taken at longer relaxation delay showed no evidence for differential relaxation. Owing to the limited amount of sample recovered from the shock experiments, the 3.2 mm probe assembly was used. For these smaller samples, the <sup>29</sup>Si experiments used 4 μs pulses (90°), 10–12 kHz spinning rates, and relaxation delays of between 2 and 10 s, which were chosen for each sample to be long enough to avoid differential relaxation effects. The <sup>27</sup>Al and <sup>23</sup>Na SP/MAS NMR spectra were collected using a 500 MHz (11.7 T) Varian Infinity Plus spectrometer (Varian, Inc., Palo Alto, California, U.S.A.) operating at 130.3 (<sup>27</sup>Al) or 132.3 (<sup>23</sup>Na) MHz with the sample spinning at 20 kHz in 3.2 mm rotors. The

acquisition parameters consisted of 0.5 μs pulses (50 kHz RF field) and 2 s relaxation delays, which correspond to uniform excitation and full relaxation of the central transition. For the shocked kaolinite samples, additional <sup>27</sup>Al spectra were acquired with a 700 MHz (16.4 T) Bruker spectrometer (Bruker Corporation of Billerica, Massachusetts, U.S.A.) located in the Stony Brook University Center for Structural Biology. These higher magnetic field spectra showed significantly reduced peak widths, compared to the data acquired at 11.7 T, for <sup>27</sup>Al signals dominated by second-order quadrupolar effects. The acquisition parameters included a 0.5 μs single-pulse excitation, 2 s relaxation delay, and 25 kHz spinning rate. Estimated relative abundances of 4-, 5-, and 6-coordinated Al in the impact shocked kaolinite were obtained by fitting both the 500 and 700 MHz spectra with the same set of uncorrelated distributions of NMR parameters (d'Espinose de Lacaillerie *et al.*, 2008).

## RESULTS

#### *NMR spectroscopy of shocked kaolinite and saponite*

Solid-state NMR spectra were acquired for shocked kaolinite and saponite to provide information on structural change in terms of the short-range bonding environments of primarily Si and Al in the tetrahedral and octahedral sheets, respectively. For comparison, the spectra of samples subjected to thermal dehydration (calcination) at constant temperature were also obtained. For Si, the primary short-range structural information is in terms of the polymerization state of the silicate tetrahedra, for which the standard notation  $Q^m$  was used, where  $Q$  denotes Si in 4-coordination to oxygen (tetrahedral Si) and  $m$  represents the number of silicate oxygens bonded to other tetrahedrally coordinated cations ( $0 \leq m \leq 4$ ). The <sup>29</sup>Si chemical shift is well established as decreasing by approximately 10 ppm with each increment in  $m$  (Engelhardt and Michel, 1987). In addition, for aluminosilicates the <sup>29</sup>Si chemical shift is sensitive to substitution of Al in adjacent tetrahedra, which is indicated by the notation  $Q^m(nAl)$ , where  $n$  is the number of connected tetrahedra occupied by Al ( $0 \leq n \leq m$ ). Each increase of  $n$  has been shown to increase the <sup>29</sup>Si chemical shift by approximately 4–5 ppm (Engelhardt and Michel 1987). The most readily available information from <sup>27</sup>Al NMR is the coordination number, with well established and non-overlapping chemical shift ranges for Al bonded to oxygen in silicates in tetrahedral 4-coordination (Al(4), +80 to +60 ppm); 5-coordination (Al(5), +40 to +30 ppm); and octahedral 6-coordination (Al(6), +20 to -10 ppm) (Smith, 1993).

Kaolinite <sup>27</sup>Al NMR spectra after impacts up to 39.6 GPa, compared to saponite <sup>27</sup>Al NMR spectra after impacts in the same pressure range (Figure 1), showed that each of these clay mineral species experienced

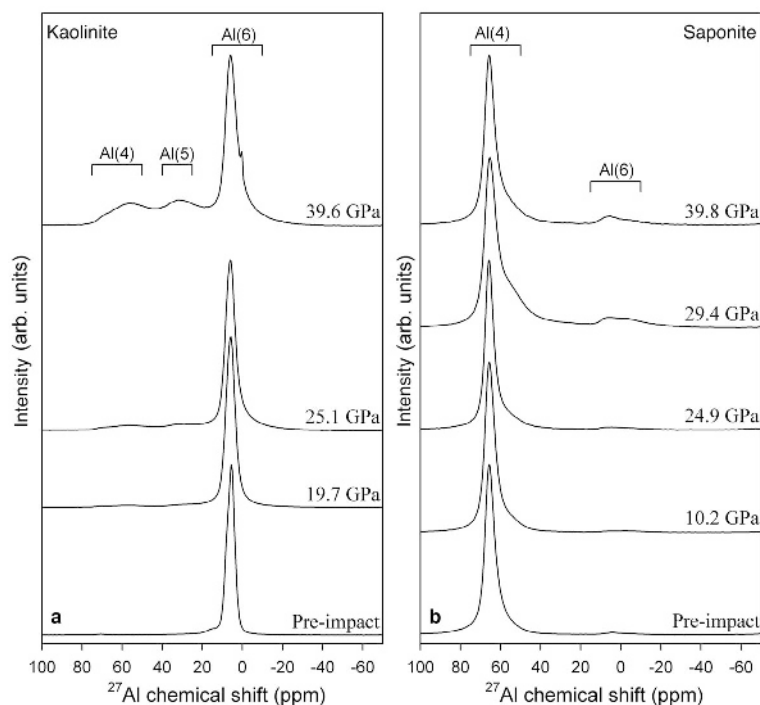


Figure 1. Comparison of the  $^{27}\text{Al}$  NMR spectra of kaolinite (a) and saponite (b) after experimental impacts at peak pressures up to  $\sim 40$  GPa.

different degrees of structural deformation as a result of exposure to experimental impact shock. Unshocked kaolinite had an NMR spectrum consistent with previous work (Hayashi *et al.*, 1992) with nearly all of the Al in the sample occupying the octahedral sheet. The predominant NMR peak (+5 ppm) had a chemical shift corresponding to that of 6-coordinated Al, except for a small (0.5% Al) peak consistent with tetrahedral Al near 71 ppm. A similar minor peak has been reported for kaolinite from this and other localities (*e.g.* Hayashi *et al.*, 1992; Newman *et al.*, 1994) and has been attributed to either an impurity phase or a small amount of Al substitution in the tetrahedral sheet. In the case of KGa-1b, an Al-bearing impurity has not been previously reported (*e.g.* Pruetz and Webb, 1993), but substitution in the tetrahedral sheet would give rise to a  $\text{Q}^3(1\text{Al})$  peak in the  $^{29}\text{Si}$  NMR spectrum of pre-impact kaolinite that was not observed (Figure 2a). After impacts up to 39.6 GPa, nearly one-half of the Al ( $47 \pm 5\%$ ) transitioned to 4- and 5-coordinated sites yielding peaks near +55 and +30 ppm, respectively (Figure 1a). In contrast, nearly all of the Al signal from the unaltered saponite sample arises from 4-coordinated Al in the tetrahedral sheet as has been reported previously for natural and synthetic saponites (Woessner, 1989). A small peak for 6-coordinated Al was observed near +5 ppm from Al substitution in the octahedral sheet, representing  $\sim 2\%$  of the Al in the sample (Woessner, 1989; Sanz *et al.*, 2015). After experimental impacts up to 39.8 GPa, the width of the tetrahedral Al peak increased slightly, implying

minor site distortion, and an additional fraction (up to  $9 \pm 2\%$ ) of the total Al transitioned to 6-coordinated Al as shown by an increase in the intensity of the +5 ppm peak (Figure 1b). Generally, the  $^{27}\text{Al}$  NMR spectrum of post-impact saponite showed less evidence for structural deformation compared to that observed for kaolinite.

Results for  $^{29}\text{Si}$  NMR experiments also showed evidence for more deformation of the kaolinite structure compared with saponite (Figure 2). For kaolinite, the signal for  $\text{Q}^3$  Si in the tetrahedral sheet at  $-91$  ppm (Magi *et al.*, 1984; Hayashi *et al.*, 1992) became broader and its intensity decreased with increasing impact pressure as significant fractions of the Si transitioned to framework-like  $\text{Q}^4$  sites. This transition produced a broad peak centered near  $-100$  ppm that accounted for  $32 \pm 5\%$  of the Si at 25.1 GPa and  $55 \pm 5\%$  at 39.6 GPa (Figure 2a). Both the  $^{27}\text{Al}$  and  $^{29}\text{Si}$  data indicated that about one-half of the sample retained kaolinite-like local structure after being subjected to shock pressures of 39.6 GPa and that the changes approached in a partial manner those observed in previous studies for thermal transformations to metakaolinite (Rocha and Klinowski, 1990a, 1990b; Massiot *et al.*, 1995; Rocha, 1999). In contrast, all of the Si in saponite retained tetrahedral sheet-like polymerization up to 39.8 GPa (Figure 2b). The unaltered sample yielded peaks at  $-95.5$  and  $-90.4$  ppm for, respectively,  $\text{Q}^3(0\text{Al})$  and  $\text{Q}^3(1\text{Al})$  Si in the tetrahedral sheet (Lipsicas *et al.*, 1984; Weiss *et al.*, 1987; Sanz *et al.*, 2015). The main effect of increasing shock pressure was an increase in the widths

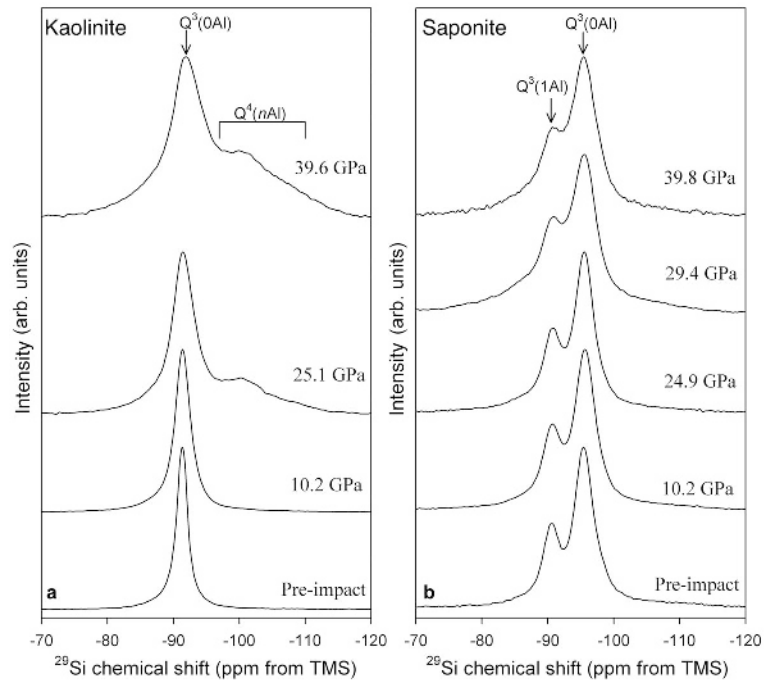


Figure 2. Comparison of the  $^{29}\text{Si}$  NMR spectra of kaolinite (a) and saponite (b) after experimental impacts at peak pressures up to  $\sim 40$  GPa.

of the main peaks. These peaks remain partially resolved up to 39.8 GPa, although broadened tails extending toward high and low frequency suggested that some Si sites were more strongly deformed than others.

The  $^{23}\text{Na}$  NMR spectra for pre- and post-impact saponite (Figure 3) confirmed the structural integrity of saponite after experimental impacts. The primary saponite  $^{23}\text{Na}$  NMR peak was consistent with Na(I) in a complex with water molecules in the saponite interlayer (Sanz *et al.*, 2015) and this feature remained largely unchanged after impacts up to 39.8 GPa. The main differences among the spectra can be attributed to differences in hydration state (Laperche *et al.*, 1990), which we did not attempt to control during these experiments. The narrow feature near +7 ppm in the spectrum of the 29.4 GPa sample is an exception and arises from a contaminant of unknown origin, likely NaCl (*e.g.* Cheetham *et al.*, 1986; Hayashi and Hayamizu, 1990), which was probably introduced during sample preparation and washing for NMR analysis. No other evidence of this halite contaminant was observed using any other analytical technique.

#### *NMR spectroscopy of thermally altered kaolinite and saponite*

The NMR spectra of heat-treated kaolinite (Figures 4a and 5a) showed nearly complete transformation at 500°C of the layered  $\text{Q}^3$  silicate polymerization to a  $\text{Q}^4$  framework-like structure, and of the octahedral Al to principally 4- and 5-coordination. For heat-treated saponite, the NMR spectra (Figures 4b and 5b) showed

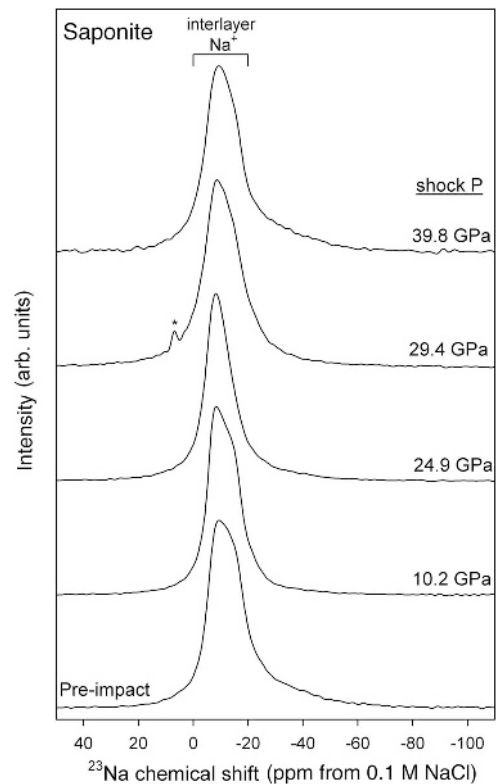


Figure 3.  $^{23}\text{Na}$  NMR spectra of saponite after experimental impacts up to 39.8 GPa peak pressure. \* A peak at 7 ppm chemical shift in the sample exposed to a peak impact pressure of 29.4 GPa arose from a contaminant of unknown origin, likely NaCl.



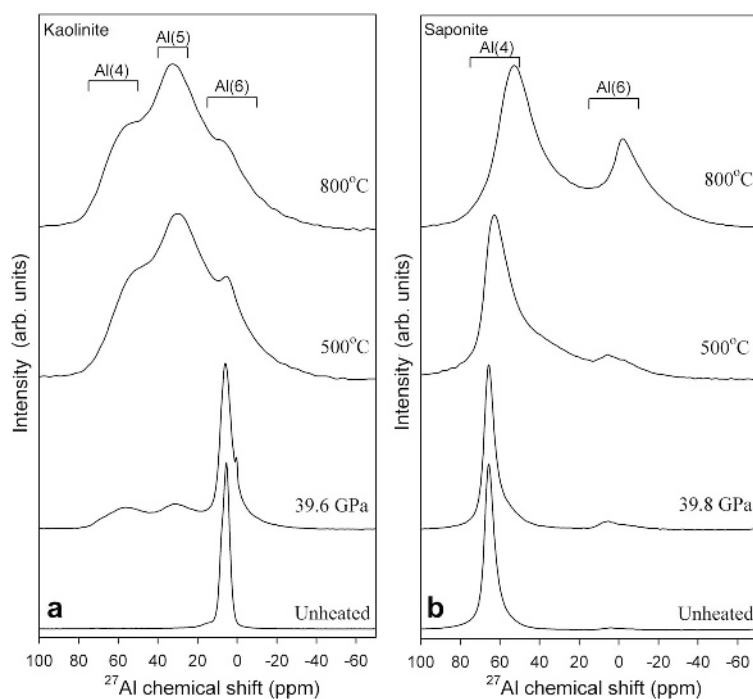


Figure 4. Comparison of  $^{27}\text{Al}$  NMR spectra of thermally altered kaolinite (a) and saponite (b).  $^{27}\text{Al}$  NMR of post-impact kaolinite and saponite are included for comparison.

that thermal alteration initially caused distortion of the tetrahedral sheet, indicated by a small peak shift and broadening of the signals from primary saponite tetra-

hedral cations (up to 500°C). At higher temperatures ( $T = 800^\circ\text{C}$ ), the eventual emergence of a pyroxene-like phase, characterized by primarily  $\text{Q}^2$  silicate polymer-

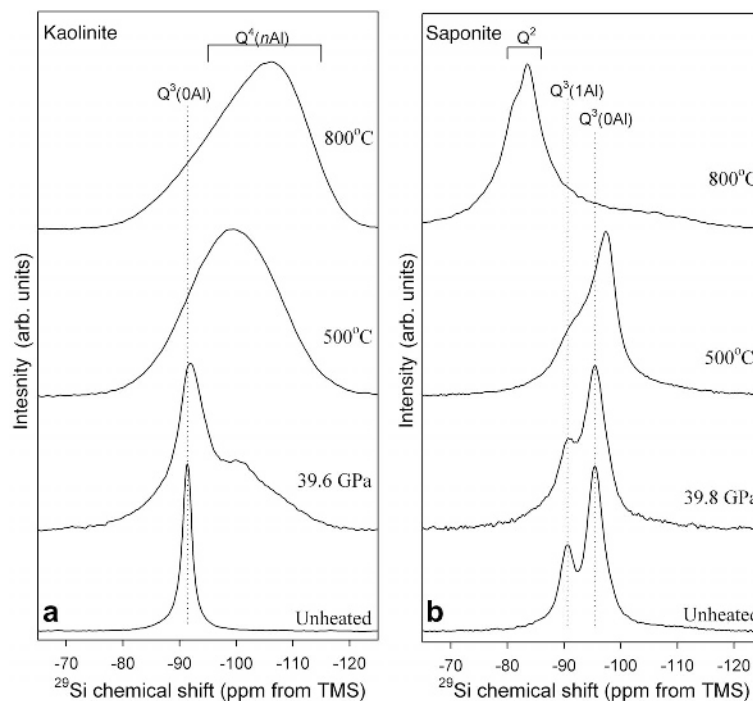


Figure 5. Comparison of  $^{29}\text{Si}$  NMR spectra of thermally altered kaolinite (a) and saponite (b).  $^{29}\text{Si}$  NMR spectra of post-impact kaolinite and saponite are included for comparison.

ization, and of an amorphous or poorly crystalline silica-rich phase (broad  $^{29}\text{Si}$  peak centered near  $-101$  ppm; Figure 4b) distinct from saponite was observed. In contrast, shock processes resulted in mainly modest peak broadening of the saponite Si and Al  $\text{Q}^3$  peaks, and did not appear to produce significant amounts of secondary phases, even after experimental impacts at peak pressures of up to 39.8 GPa (Figures 4 and 5, peak-pressure post-impact spectra reprinted for easy comparison).

#### VNIR spectroscopy of shocked kaolinite and saponite

VNIR spectroscopy of shocked kaolinite (Figures 6a) confirmed the NMR results and showed greater evidence of structural deformation in kaolinite than saponite. The pre-impact kaolinite VNIR reflectance spectrum was consistent with previous work on well crystalline kaolinite samples. OH-group combination and overtone bands dominate the kaolinite reflectance spectrum in the VNIR wavelength region. Between 1.25–1.45  $\mu\text{m}$  ( $8000$ – $6896$   $\text{cm}^{-1}$ ), two strong bands were resolved at 1.39  $\mu\text{m}$  ( $7176$   $\text{cm}^{-1}$ ) and 1.42  $\mu\text{m}$  ( $7065$   $\text{cm}^{-1}$ ) corresponding to the  $2\nu_{\text{OH}}$  overtones of  $\text{Al}_2\text{OH}$  stretching fundamentals (Petit *et al.*, 1999 and citations therein). The other smaller bands in this region (1.36  $\mu\text{m}$ , 1.31  $\mu\text{m}$ , and 1.24  $\mu\text{m}$ ) have not been clearly assigned, but arise from overtones and combinations of the fundamental  $\text{Al}_2\text{OH}$  group bends and stretches. The presence of multiple small bands in this region, however, has previously been suggested as indicative of a well crystallized sample (Clark, 1999). The small band at 0.97  $\mu\text{m}$  ( $10335$   $\text{cm}^{-1}$ ) can be attributed either to the 2<sup>nd</sup> overtone of the stretching fundamental modes of  $\text{Al}_2\text{OH}$  or to Fe(II) substitution (*e.g.* Petit *et al.*, 1999). Structural Fe has been observed by IR spectroscopy in

KGa-2, but not KGa-1b (*e.g.* Madejová and Komadel, 2001). The strong band at 1.91  $\mu\text{m}$  ( $5236$   $\text{cm}^{-1}$ ) arises in the spectrum of kaolinite from the presence of adsorbed water and disappears under vacuum (Delineau *et al.*, 1994).

Between 2.1–2.5  $\mu\text{m}$  ( $4762$ – $4000$   $\text{cm}^{-1}$ ), the combinations and overtones of  $\text{Al}_2\text{OH}$  fundamentals appear, overlapping with one another and with bands from other parts of the kaolinite structure. The asymmetric doublet centered at 2.21  $\mu\text{m}$  ( $4525$   $\text{cm}^{-1}$ ) arises from the combination of one  $\text{Al}_2\text{OH}$  stretching and one  $\text{Al}_2\text{OH}$  bending fundamental. The nearby weak band at 2.11  $\mu\text{m}$  ( $4730$   $\text{cm}^{-1}$ ) is thought to be a combination of internal  $\text{AlAlOH}$  stretching ( $3620$   $\text{cm}^{-1}$ ; 2.76  $\mu\text{m}$ ) and the SiO stretching fundamental ( $\sim 1100$   $\text{cm}^{-1}$ ). The small bands observed between 2.32–2.44  $\mu\text{m}$  ( $4300$ – $4100$   $\text{cm}^{-1}$ ) have been previously assigned to  $\text{Al}_2\text{OH}$  stretching fundamentals in combination with kaolinite lattice vibrations (Petit *et al.*, 1999 and citations therein). The main effect of increased peak experimental impact pressures on the reflectance spectrum of kaolinite was loss of detail in the smaller spectral features. Such changes have been previously associated with decreased crystallinity (Clark, 1999). Similar spectral changes in another dioctahedral phyllosilicate, nontronite, have also been related to structural deformation in the octahedral sheet (*e.g.* Friedlander *et al.*, 2015). Such a hypothesis is supported by the changes described above for the  $^{27}\text{Al}$  NMR spectra of shocked kaolinite.

In contrast to the VNIR reflectance spectra of shocked kaolinite, the VNIR reflectance spectra of shocked saponite still showed strong, detailed features up to peak impact pressures of 39.8 GPa (Figure 6b). The pre-impact VNIR reflectance spectrum of saponite was

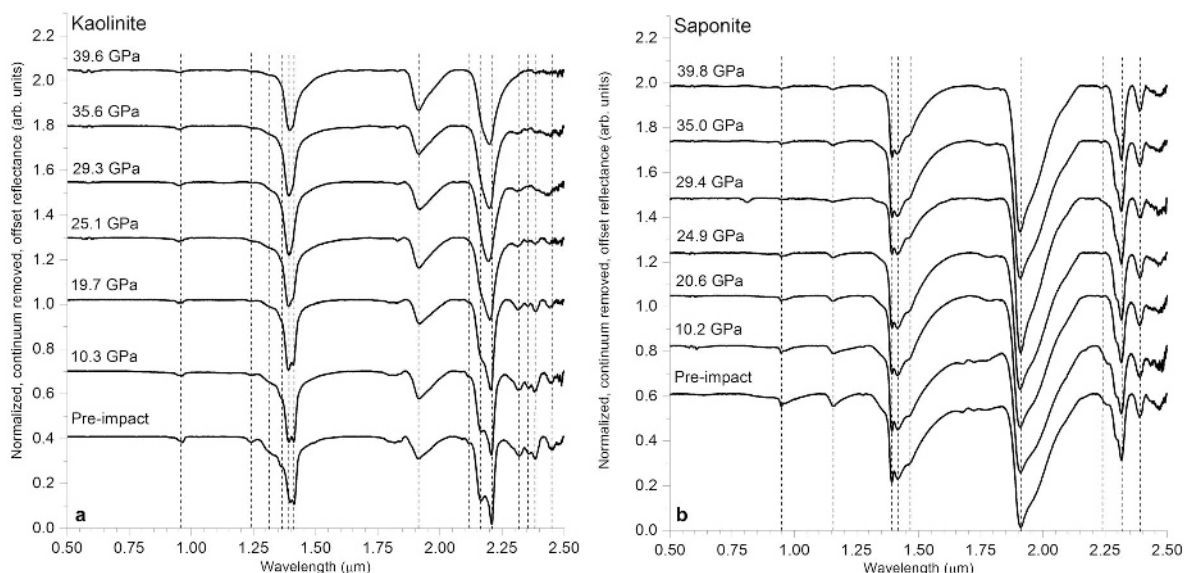


Figure 6. Normalized, continuum removed, VNIR reflectance spectra of kaolinite (a) compared to saponite (b). Dashed lines refer to spectral features discussed in detail in the text. Band centers given in the text are in both wavelength ( $\mu\text{m}$ ) and wavenumber ( $\text{cm}^{-1}$ ).

consistent with previous work and was, similar to kaolinite, dominated by octahedral sheet hydroxyl group combination and overtone bands (Clark *et al.*, 1999; Bishop *et al.*, 2002a, 2008a, 2008b). The  $\text{Mg}_3\text{OH}$  stretching and bending combination doublet centered at  $2.31 \mu\text{m}$  ( $4329 \text{ cm}^{-1}$ ) and the  $\text{Mg}_3\text{OH}$  bending overtone centered at  $2.39 \mu\text{m}$  ( $4184 \text{ cm}^{-1}$ ) did not change either normalized intensity or band center, even after experimental impacts at pressures up to 39.8 GPa (Clark *et al.*, 1999). Some variability was observed for bands in the  $2.23\text{--}2.27 \mu\text{m}$  region ( $4484\text{--}4405 \text{ cm}^{-1}$ ). The shoulder feature at  $2.25 \mu\text{m}$  ( $4444 \text{ cm}^{-1}$ ) and the weak band at  $2.23 \mu\text{m}$  ( $4484 \text{ cm}^{-1}$ ) correspond to octahedral  $\text{AlMgOH}$  and  $\text{AlFeOH}$  combination bands (Bishop *et al.*, 2002a, 2002b, 2008a, 2008b), respectively, and showed the greatest variability between samples. SapCa-2 contains  $<1\%$  Fe(III) (Post, 1984), but does contain Al substituted in the octahedral sheet, as shown by NMR spectroscopy (Figure 1b). Variability in these bands may thus arise from compositional and substitutional variability, rather than impact-induced structural deformation, in particular the amount of Al substitution in the saponite octahedral sheet. Two large, complex features exist in the saponite reflectance spectrum between  $0.9\text{--}1.9 \mu\text{m}$  ( $11,111\text{--}5263 \text{ cm}^{-1}$ ). The first, centered at  $1.3 \mu\text{m}$  ( $7692 \text{ cm}^{-1}$ ), arises from the second overtones of both  $\text{Mg}_3\text{OH}$  and structural  $\text{H}_2\text{O}$  stretching fundamentals. The second large band at  $1.91 \mu\text{m}$  ( $5236 \text{ cm}^{-1}$ ), by comparison to similar results for montmorillonite (Bishop *et al.*, 1994), likely arises from the combination of interlayer  $\text{H}_2\text{O}$  bending and stretching vibrations. The strength and detail of the reflectance features observed in the saponite VNIR spectrum after impacts up to 39.8 GPa were consistent with saponite retaining a

largely unaltered octahedral sheet structure, even after high pressure experimental impacts. This is in marked contrast to results for kaolinite and nontronite (*e.g.* Friedlander *et al.*, 2015).

#### MIR emissivity spectroscopy of shocked kaolinite and saponite

The MIR emissivity spectra of phyllosilicates reveal structural information about silicate bonding in the tetrahedral sheet, superposed with hydroxyl group vibrations from the octahedral sheet (Clark, 1999; Bishop *et al.*, 2008b). Similar to the VNIR reflectance spectrum of kaolinite, spectral contrast between features in the emissivity spectrum of kaolinite decreased with increasing peak experimental impact pressure (Figure 7a). The emissivity spectrum of pre-impact kaolinite was consistent with previous spectroscopic work on other kaolinite samples, such as KGa-1 (Petit *et al.*, 2004; Bishop *et al.*, 2008b), as well as previous analyses of KGa-1b (Pruett and Webb, 1993). The asymmetric triplet centered at  $1060 \text{ cm}^{-1}$  ( $9.43 \mu\text{m}$ ) is attributed to  $\text{SiO}$  stretching fundamental vibrations ( $1130 \text{ cm}^{-1}$ ,  $1060 \text{ cm}^{-1}$ , and  $1010 \text{ cm}^{-1}$ ). At the low-frequency edge of this range, some overlap may exist with superposed  $\text{Al}_2\text{OH}$  deformation vibrations (Clark, 1999; Michalski *et al.*, 2006). The bands at  $940 \text{ cm}^{-1}$  and  $910 \text{ cm}^{-1}$  ( $10.64\text{--}11.00 \mu\text{m}$ ) are attributed to the  $\text{Al}_2\text{OH}$  bending vibrations of inner-surface and inner hydroxyl groups (Madejová and Komadel, 2001), respectively. At lower frequencies,  $\text{SiO}$  bending vibrations occur in the kaolinite spectrum. The three bands at  $555 \text{ cm}^{-1}$  ( $18.0 \mu\text{m}$ ),  $475 \text{ cm}^{-1}$  ( $21.0 \mu\text{m}$ ), and  $425 \text{ cm}^{-1}$  ( $23.5 \mu\text{m}$ ) have all been attributed to the various bending modes of  $\text{SiO}$  in the tetrahedral sheet of kaolinite (*e.g.* Farmer, 1968; Bishop *et al.*, 2002a, 2002b).

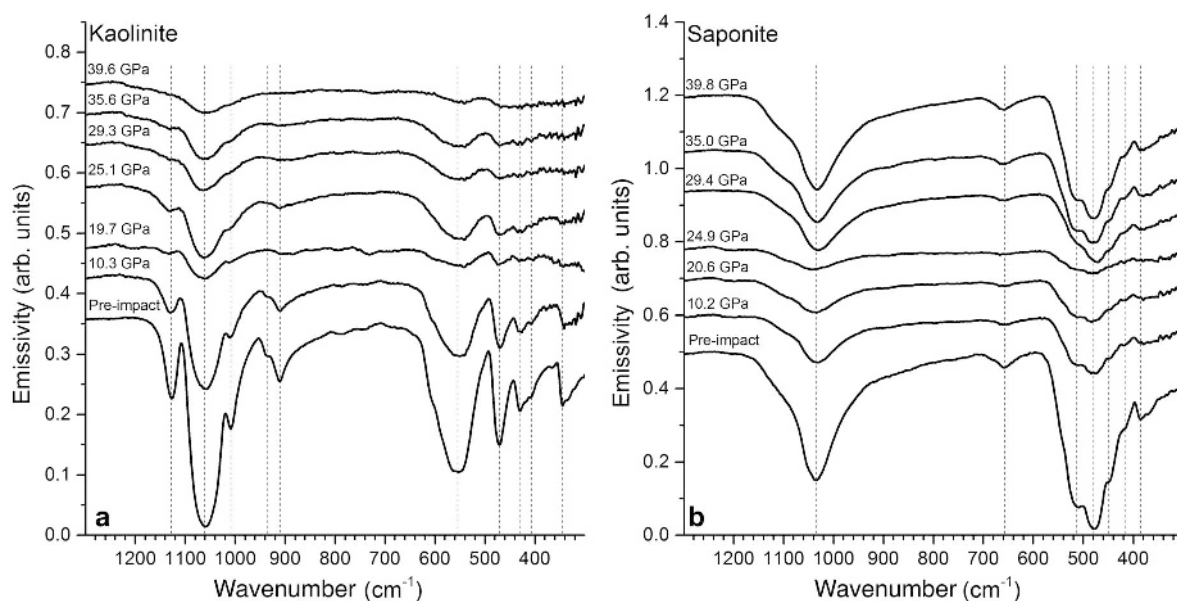


Figure 7. MIR emissivity spectra of post-impact kaolinite (a) compared to saponite (b).

Below this frequency range, bands, such as the broad band at  $340\text{ cm}^{-1}$  ( $29.4\text{ }\mu\text{m}$ ), are related to combinations of lattice vibrations and  $\text{Al}_2\text{OH}$  deformations (Farmer, 1968).

Similar to the effects observed in the VNIR reflectance spectra of kaolinite, experimental impacts at high pressures produced samples with emissivity spectra that showed reduced spectral contrast and typically lacked small features. After impacts up to  $39.6\text{ GPa}$ , no minor features were observed and only broad  $\text{SiO}$  stretching and bending features centered at  $1060\text{ cm}^{-1}$  and  $555\text{ cm}^{-1}$ , respectively, remained. Similar results for the dioctahedral smectite nontronite have been interpreted as reflective of structural deformation and partial amorphization of the tetrahedral sheet (*e.g.* Friedlander *et al.*, 2015). This interpretation is also supported by  $^{29}\text{Si}$  NMR results from shocked kaolinite in which roughly half of the Si transitioned into framework-like  $\text{Q}^4$  sites after experimental impacts at  $39.6\text{ GPa}$  peak pressure.

In contrast to the results reported for kaolinite, the MIR emissivity spectrum of saponite remained largely consistent with pre-impact saponite up to peak impact pressures of  $39.8\text{ GPa}$  (Figure 7b). The post  $24.9\text{ GPa}$  peak impact pressure sample was one exception. Spectral signal and contrast in emissivity spectra are related to physical interactions between sample grains, in addition to structural and mineralogical changes (*e.g.* Michalski *et al.*, 2005). Given that spectral results observed for this sample using other techniques showed no substantial differences relative to other saponite samples, the difference in emissivity signal probably resulted from physical differences between the  $24.9\text{ GPa}$  sample and the other saponite samples, rather than structural deformation. The saponite tetrahedral  $\text{SiO}$  stretching band center occurred at a slightly lower frequency than that observed for kaolinite ( $1040\text{ cm}^{-1}$ ;  $9.62\text{ }\mu\text{m}$ ). It also had fewer secondary bands because the  $\text{Mg(II)OSi}$  deformation absorption is not uniquely identifiable in trioctahedral smectites (Michalski *et al.*, 2005 and citations therein). The sharp feature at  $657\text{ cm}^{-1}$  ( $15.2\text{ }\mu\text{m}$ ) has previously been assigned to the  $\text{Mg}_3\text{OH}$  bending vibration (Kloprogge and Frost, 2001). The overlapping bands observed between  $580\text{--}360\text{ cm}^{-1}$  ( $17.2\text{--}27.8\text{ }\mu\text{m}$ ) arise from tetrahedral  $\text{SiO}$  bends superposed on  $\text{Mg}_2\text{AlOH}$  and  $\text{Mg}_3\text{OH}$  bends and translations with hydroxyl group bands occurring at higher frequencies than the  $\text{SiO}$  bending bands (Kloprogge and Frost, 2001). The  $\text{Mg}_3\text{OH}$  bending band at  $657\text{ cm}^{-1}$  broadened in some saponite emissivity spectra, but was still present after experimental impacts at the highest peak pressure,  $39.8\text{ GPa}$ .

#### *MIR ATR spectroscopy of shocked kaolinite and saponite*

ATR spectroscopy approximates infrared absorption spectroscopy (Fahrenfort, 1961) and ATR spectra show well resolved peaks that are useful for deriving structural

information from regions of complex and overlapping bands. The ATR spectra of post-impact kaolinite (Figure 8a) showed structural deformation in both the tetrahedral and octahedral sheets. Band assignments for the ATR spectrum of pre-impact kaolinite between  $1300\text{--}450\text{ cm}^{-1}$  ( $7.69\text{--}22.2\text{ }\mu\text{m}$ ) are the same as those for the pre-impact kaolinite emissivity spectrum and have been previously investigated and assigned (*e.g.* Madejová and Komadel, 2001). The MIR OH stretching region of pre-impact kaolinite showed four close, but distinct, bands between  $3700\text{--}3620\text{ cm}^{-1}$  ( $2.7\text{--}2.76\text{ }\mu\text{m}$ ). The strong, sharp band at  $3620\text{ cm}^{-1}$  has previously been assigned to inner  $\text{Al}_2\text{OH}$  group stretching vibrations. The other three bands remain controversial and have not been definitively assigned, but are agreed to be  $\nu\text{Al}_2\text{OH}$  vibrations (Petit *et al.*, 2004 and citations therein). With increasing peak impact pressure, these bands broaden into a single feature centered at  $\sim 3650\text{ cm}^{-1}$  ( $2.74\text{ }\mu\text{m}$ ) and are eventually not detected in the ATR spectrum of kaolinite after experimental impacts at  $35.6\text{ GPa}$  and higher. Similar to the results observed for the MIR emissivity spectrum of post-impact kaolinite, the detail and spectral contrast of the  $1500\text{--}450\text{ cm}^{-1}$  region of the post-impact kaolinite ATR spectra decreased with increasing peak impact pressure. At the highest peak impact pressure, only broad  $\text{SiO}$  stretching ( $\sim 1100\text{ cm}^{-1}$ ) and  $\text{SiO}$  bending ( $\sim 480\text{ cm}^{-1}$ ) features were observed.

In contrast, the post-impact ATR spectra of saponite resembled pre-impact saponite up to the highest experimental peak impact pressure ( $39.8\text{ GPa}$ ). In particular, both the sharp  $\text{Mg}_3\text{OH}$  stretching ( $3680\text{ cm}^{-1}$ ;  $2.72\text{ }\mu\text{m}$ ) and  $\text{Mg}_3\text{OH}$  bending ( $657\text{ cm}^{-1}$ ;  $15.2\text{ }\mu\text{m}$ ) bands persisted throughout the series with only slight broadening and no changes in their observed band centers. Generally, results produced by VNIR and MIR spectroscopic analyses of post-impact kaolinite and saponite followed similar trends to those reported for NMR spectroscopy, with trioctahedral saponite showing less susceptibility to structural deformation than dioctahedral kaolinite. The results reported for kaolinite were similar to results that have been previously reported for the dioctahedral smectite nontronite (*e.g.* Friedlander *et al.*, 2015).

## DISCUSSION

### *NMR spectroscopy of local-scale structural deformation*

The use in this study of NMR spectroscopy, which is a reproducible and extremely sensitive probe of atomic-scale structural disorder in Si-bearing phases, is an important addition to the current understanding of structural change in silicate phases post-shock. This technique has thus far been applied primarily to tectosilicates (quartz, feldspar) after experimental impacts (Cygan *et al.*, 1992; Fiske *et al.*, 1998) or as a test of ancient impact hypotheses (*e.g.* along the K/Pg boundary) through comparisons of experimental and naturally shocked tectosilicate samples (Boslough *et al.*,

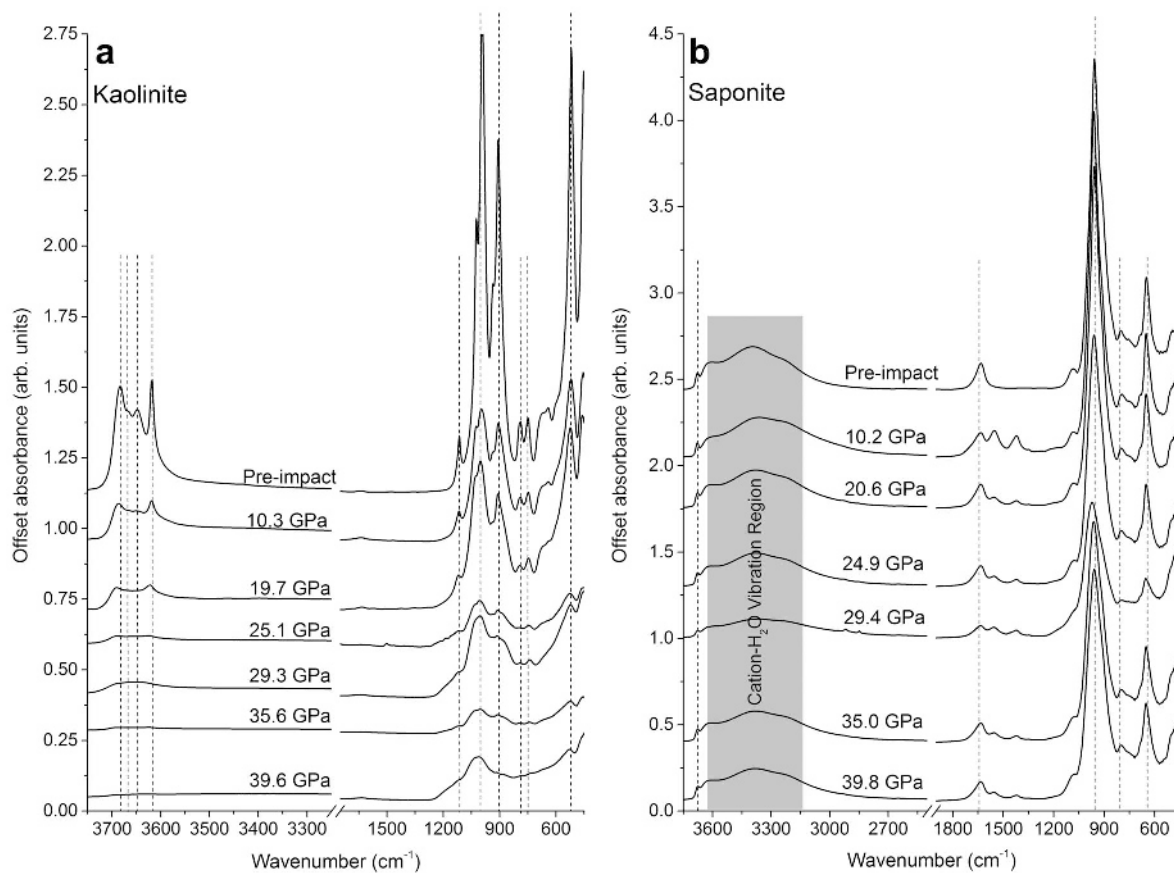


Figure 8. MIR ATR spectra of post-impact kaolinite (a) compared to saponite (b).

1995). In the present study, NMR provided unique information about changes to the bonding environments in both the octahedral and tetrahedral sheets of shocked phyllosilicate species, especially in comparison to thermal alteration (Figures 4 and 5).

The short-range structural changes in kaolinite brought about by impacts at the highest shock pressures appeared qualitatively similar to those caused by thermal alteration (Rocha and Klinowski, 1990b; Massiot *et al.*, 1995; Rocha, 1999). The extent, however, was less pervasive, retaining some regions of apparent kaolinite-like local structure, more similar to results for flash calcined kaolinite (Slade and Davies, 1991; Slade *et al.*, 1991; Meinhold *et al.*, 1992, 1993). The minor structural changes produced in saponite by impacts at the highest shock pressures (Figures 1, 2, and 3) were in stark contrast to the production of much more obvious changes in shocked kaolinite. Thermally altered saponite retained more original structure at 500°C than kaolinite (Figures 4 and 5). After calcination up to 800°C, however, it converted to an enstatite-dominated secondary phase (Kulbicki, 1959; Che *et al.*, 2011). These results can be interpreted as partially supporting the hypothesis that trioctahedral phyllosilicates are more resistant to structural deformation as a response to stress,

either shock or thermal alteration. They also showed that the input of sufficient energy could eventually produce structural deformation in trioctahedral phyllosilicates.

The saponite sample analyzed after a 29.4 GPa impact showed an anomalously large increase in the tetrahedral Al peak width coupled with the appearance of a singular and more prominent shoulder near 55 ppm (Figure 1), which suggested either that larger structural distortions occurred in this sample or that secondary phases were produced in this experiment. This demonstrated potential variability in structural deformation after impacts, even among samples of the same phyllosilicate. Further spectroscopic evidence for long-range structural breakdown, however, was not observed for this sample using other techniques. This suggested that these results might be driven by initial structural variability between saponite samples, rather than impact alteration. Overall, the trend of the results presented here and in comparison with previous work on nontronite (*e.g.* Gavin *et al.*, 2013; Friedlander *et al.*, 2015) implied that dioctahedral phyllosilicates may be more susceptible to structural deformation after experimental impacts than trioctahedral phyllosilicates.

The <sup>27</sup>Al NMR spectrum of unaltered kaolinite was consistent with all structural Al occupying 6-coordinated

sites in the octahedral sheet. After experimental impacts up to 39.6 GPa, nearly half ( $47 \pm 5\%$ ) of the Al had transitioned to 4- and 5-coordinated sites (Figure 1a). In contrast, the 4-coordinated  $^{27}\text{Al}$  NMR peak of unaltered saponite, consistent with Al substituting for Si in the tetrahedral sheet, was largely unaltered by experimental impacts up to 39.8 GPa. At higher pressures, a higher intensity was observed for the  $^{27}\text{Al}$  NMR peak consistent with 6-coordinated Al in the saponite octahedral sheet. Three possible interpretations for this result are hypothesized. (1) The saponite tetrahedral sheet was partially structurally deformed, driving some Al into the octahedral sheet. This is unlikely because mobilizing cations requires a large amount of energy. (2) The unaltered saponite sample(s) exposed to experimental impacts at higher peak pressures had larger proportions of aluminum in their octahedral sheets. (3) Impact shock generated secondary phases distinct from saponite. By comparison with thermal alteration, this secondary phase is likely to be an enstatite-rich phase, possibly in combination with amorphous silica (*e.g.* Kulbicki, 1959). The formation of an Mg-rich secondary phase may result in enrichment of Al in the saponite octahedral sheet or simply decreased intensity of the structurally normal saponite NMR peaks. This third interpretation is consistent with NMR spectra from impact-altered saponite that showed results similar to those observed for thermal alteration, but on a smaller scale. Localized heating at grain boundaries during the shock-recovery experiments may have produced enough thermally altered saponite to explain these results. Nonetheless, the similarity observed in the  $^{23}\text{Na}$  NMR spectra of the pre-impact and high-pressure post-impact saponite indicated that overall shock deformation slightly disrupted the saponite layered structure, without inducing total loss of the sample's long-range structural order.

#### *Structural deformation in shocked dioctahedral versus trioctahedral phyllosilicates*

The similarity of the deformation observed for kaolinite after impacts at moderate peak-pressures (*e.g.* 25.1 GPa) to the deformation of nontronite after experimental impacts at similar (*e.g.* 25.2 GPa) pressures (Friedlander *et al.*, 2015) suggested that susceptibility to impact-induced structural deformation is not dependent on the presence of a hydrated interlayer. In fact, impact-induced long- and short-range structural deformation observed in both nontronite and kaolinite, but much less significantly in post-impact saponite, instead suggested that dioctahedral minerals may be more susceptible to deformation than trioctahedral minerals. One hypothesis that explains this result is that the observed differences may be driven by the availability of vacancies in the octahedral sheets of dioctahedral phyllosilicates that are not present in the octahedral sheets of trioctahedral phyllosilicates. This hypothesis has been previously suggested to explain

observed differences in the hydrothermal reactivity of trioctahedral (less reactive) and dioctahedral (more reactive) smectites (Eberl *et al.*, 1978). Indeed, previous researchers have suggested generally that smectite stability increases when all octahedral sites are fully occupied (Sand and Ames, 1957; Ames and Sand, 1958). Careful comparisons of the shock responses of additional phyllosilicate species may help to prove or disprove this. Unfortunately, currently available data on the effects of shock on phyllosilicates is rather sparse and limited to a few key minerals.

The effects of experimental impacts between 10–40 GPa on the structure and spectroscopy of nontronite, for example, have been previously reported in detail (Friedlander *et al.*, 2015). In summary, nontronite responds to shock through structural degradation beginning with the deformation of the octahedral sheet, rapid total degradation of the tetrahedral sheet, and eventual emergence of an amorphous Fe-Al/Si-OH secondary phase. This interpretation was supported by data from VNIR reflectance, MIR emissivity and ATR, Mössbauer, and Raman spectroscopy and confirmed by XRD and transmission electron microscopy (TEM). Other researchers have found that experimental impacts more strongly affected the MIR spectra and XRD patterns of nontronite than the VNIR spectra and reported few impact-induced spectral changes in this wavelength region (*e.g.* Gavin *et al.*, 2013). Their results likely differ from those reported by Friedlander *et al.* (2015) and in this manuscript because of the relatively low peak pressures achieved in their impact experiments; 17.5 GPa was the highest peak pressure reported for their nontronite sample. Direct comparisons with these results are also complicated because Gavin *et al.* (2013) reported mostly impactor velocities and modeled peak pressures for only their nontronite and montmorillonite samples. In addition, all of the samples used by Gavin *et al.* (2013) were dominated by trivalent octahedral cations and, as a result, they reported the same general trends for shock responses in all of their samples without the strong variability between dioctahedral and trioctahedral phyllosilicates observed in the results presented here.

#### *Spectroscopy of thermal and shock alteration*

Thermal and shock alteration effects are associated and, to a large extent, inseparable in natural samples (French, 1968, 1998; Stöfler, 1972, 1974). By isolating these two processes as much as empirically possible, however, the effects of shock and thermal alteration on clay mineral structure and spectroscopy can be partly distinguished and compared. Previous research has already shown that thermal alteration produces physical and spectral properties in nontronite that differ from those produced by shock (Boslough *et al.*, 1986). The results presented here are consistent with those findings.

Previous work on the thermal alteration of hydrated phyllosilicates has shown that the resulting structural

deformation generally follows a pathway that can be broken down into steps related to the part of the phyllosilicate structure being altered. H<sub>2</sub>O adsorbed to grain surfaces is driven off first; then, at slightly higher temperatures (100°C <  $T$  < 300°C), interlayer H<sub>2</sub>O molecules are driven off from the structure. This is followed by dehydroxylation ( $T = 400^\circ\text{C}$ ), layer collapse (500°C ≤  $T$  ≤ 800°C), and the emergence at high temperatures ( $T \geq 800^\circ\text{C}$ ) of completely dehydrated secondary or amorphous phases. The thermal alteration of non-hydrated phyllosilicates generally follows a similar stepwise progression, but begins with dehydroxylation at  $T \cong 400^\circ\text{C}$ , rather than dehydration at lower temperatures (Moskowitz and Hargraves, 1984; Fitzgerald *et al.*, 1996; Carroll *et al.*, 2005; Gavin and Chevrier, 2010; Che *et al.*, 2011; Daly *et al.*, 2011; Che and Glotch, 2012). In contrast, structural deformation following impacts is more variable and does not necessarily lead to irreversible dehydration or dehydroxylation in shocked samples (*e.g.* Gavin *et al.*, 2013; Kraus *et al.*, 2013; Friedlander *et al.*, 2015). The most diagnostic changes to the VNIR reflectance spectra of impact-altered kaolinite and nontronite, for example, occur in the 2.2–2.4 μm (4545–4167 cm<sup>-1</sup>) region, which contains the Al<sub>2</sub>OH, Fe<sub>2</sub>OH, and AlFeOH vibrational combination and overtone bands that are diagnostic of the cations present in the octahedral sheet (Bishop *et al.*, 2002b, 2008a; Petit *et al.*, 2004). The collapse of the many structurally indicative features in this region into a single broad feature (Figure 6a, and Friedlander *et al.*, 2015) can be interpreted as resulting from a loss of short-range structural order in the octahedral sheet without complete dehydroxylation. Comparable structural deformation does not occur during thermal alteration without prior dehydroxylation.

The NMR results presented here further supported the hypothesis that thermal and shock alteration may proceed via different pathways and produce different structural changes in materials exposed to both processes. The NMR spectra of thermally altered and shocked kaolinite revealed that instead of the gradual change in aluminum coordination that was observed for shocked kaolinite, the aluminum in thermally altered kaolinite passed all at once into mostly 4- and 5-coordinated sites characteristic of metakaolinite (Figure 4a). The <sup>29</sup>Si NMR spectra indicated that transformation of kaolinite to amorphous metakaolinite was complete at  $T \geq 500^\circ\text{C}$  (Figure 5a). In contrast, even in the kaolinite sample shocked up to the highest peak pressure of 39.6 GPa, slightly more than half of the sample retained local kaolinite-like structure. This is consistent with a process that causes irregular, rather than stepwise, structural change. These results may also reflect the localized heating that can occur in shock-reverberation experimental samples, or the possibility that shock only imparts enough energy to partially drive mineral transitions to amorphous and/or metastable

phases. This may be due to kinetic differences between shock and thermal alteration. While shock passes nearly instantaneously through a sample, on the order of ~0.1–1 μs (Stöffler, 1972), the thermal alteration results used in this study were acquired after calcination of clay minerals over 24 h (Che *et al.*, 2011; Che and Glotch, 2012). As a result, kinetic differences between these two laboratory processes are to be expected. A similar kinetic difference exists, however, in the non-linear relationship between shock and heat in natural impact processes (French, 1968, 1998). This means that structural and spectral differences between the effects of shock and heat observed in laboratory studies are likely to be reflected in natural meteoroid impacts and should be taken into account in remote sensing data analysis.

#### *Implications for martian remote sensing*

The results presented here have potentially important implications for the analysis of remote sensing data, especially in regions that have undergone heavy impact bombardment, such as the southern highlands of Mars. They have demonstrated that spectroscopic techniques can detect the effects of shock in clay minerals, and it may therefore be possible to detect shock metamorphism on Mars from infrared data. These results have also demonstrated, however, that detections of shock metamorphism are likely to be complicated by the differing responses of structurally different minerals to shock. Two analyzed dioctahedral phyllosilicates exhibited shock effects at relatively low pressures (~25 GPa), whereas the analyzed trioctahedral clay mineral showed almost no effects up to the highest experimental impact peak pressure (~40 GPa).

Martian crater densities for large (diameter > 64 km) craters are comparable in some places to those of the lunar highlands, amounting to around one crater of this size every 10,000 km<sup>2</sup> (Hartmann and Neukum, 2001 and citations therein). Modeling results have shown that pressures > 300 GPa can be expected in impacts from meteoroids with diameters of 50 km or larger (French, 1998). Impacts of this size are rare. More than 100 craters per km<sup>2</sup> of diameter ≤ 1 km exist on the martian surface; however, many of them were produced within the last 1000 years (Hartmann and Neukum, 2001). The range of shock effects produced by such a variety of craters is likely to be large and dependent on the velocity of the impactor, the material of the impactor, and the incident target material (Rankine, 1870; Hugoniot, 1889; Gault and Heitowitz, 1963). By way of orientation, Barringer Crater (also known as Meteor Crater) in Arizona is 1.2 km in diameter and is believed to have exposed the incident surrounding materials to shock pressures of at least 160 kbars (16 GPa) or higher (Chao *et al.*, 1962). As a result, exposure to extreme shock effects is expected to be relatively rare, but likely to produce extreme effects on a

large amount of material where they do occur. In contrast, moderate shock effects (15 GPa  $\leq$  peak pressure  $\leq$  25 GPa) are likely to affect large areas of a planetary surface, but potentially less extremely. Based on the results presented here and the distribution of martian crater sizes, one likely inference is that dioctahedral phyllosilicates are likely to have been more structurally altered than trioctahedral phyllosilicates in many parts of the martian surface. As a result, shock effects may affect the interpreted ratio of dioctahedral to trioctahedral clay minerals on Mars based on IR data (*e.g.* Carter *et al.*, 2013), leading to an overestimation of the abundances of trioctahedral relative to dioctahedral phyllosilicates. Shock effects may also explain the prevalence of such ambiguous clay mineral identifications as the semi-ubiquitous and unspecified Fe/Mg-smectite identifications on the martian surface, frequently cited as the most common phyllosilicate identification on Mars by remote sensing (Mustard *et al.*, 2008; Ehlmann *et al.* 2009; Carter *et al.*, 2013).

### CONCLUSIONS

Many phyllosilicate identifications by VNIR remote sensing on Mars have been made, but not all identifications are specific and many are ambiguous. One of the most common is a non-specific Fe/Mg-smectite. Martian phyllosilicates are ancient and likely to have experienced significant alteration by meteoroid bombardment. As a result, structural deformation related to the alteration of martian phyllosilicate deposits by shock likely contributes to the remote sensing results observed for phyllosilicates on Mars, especially ambiguous remote sensing results. In contrast to previous work investigating shock effects in phyllosilicates, the experimental results presented here associate structural and spectral changes with known shock pressures, rather than impactor velocities. Computed shock pressures are more useful gauges of shock effects than impactor velocity because impactor and target materials can affect the peak shock pressures produced by impacts, even at the same impactor velocities. As a result, the work presented here provides a clearer and also more detailed picture of the effects that impacts have on phyllosilicates of various structures. Dioctahedral phyllosilicates showed greater susceptibility to structural deformation by shock, deforming at lower peak pressures and more intensely than trioctahedral phyllosilicates. On Mars, such a result implies that abundances of trioctahedral phyllosilicates may be overestimated relative to dioctahedral phyllosilicates. This may explain the prevalence of the common, undifferentiated Fe/Mg-smectite signature in martian regions with strong phyllosilicate identifications. In contrast to thermal alteration, the irregular nature of shock deformation also increases the likelihood that multiple and variable shock effects may

affect martian phyllosilicate spectral signatures in unpredictable ways. Laboratory work examining additional, and especially mixed, phyllosilicates under shock conditions and in comparison to thermal alteration may help to explain and predict these effects.

### ACKNOWLEDGMENTS

The authors thank Dr. Rampe and two anonymous reviewers whose suggestions greatly improved the structure and clarity of this manuscript. Mark Cintala conducted impact experiments at the Flat Plate Accelerator facility at Johnson Space Center. The authors are particularly grateful for his expertise and assistance in providing essential information on the techniques used, and for his work running the many experiments required to generate the data used in this manuscript. This work was funded through a NASA Mars Fundamental Research Program grant to P.I. Joseph Michalski (Grant Reference #: NNX10AM83G). All of the referenced data from the VNIR reflectance, MIR emissivity, and MIR ATR spectroscopic results are available on the Stony Brook University Vibrational Spectroscopy Laboratory homepage (<http://aram.ess.sunysb.edu/tglotch/spectra.html>).

### REFERENCES

- Abramov, O. and Kring, D.A. (2005) Impact-induced hydrothermal activity on early Mars. *Journal of Geophysical Research*, **110**, E12S09.
- Adams, J.B., Hörz, F., and Gibbons, R.V. (1979) Effects of shock-loading on the reflectance spectra of plagioclase, pyroxene, and glass. *Tenth Lunar and Planetary Science Conference*, Lunar and Planetary Institute Contribution 1576, Abstract #1001.
- Ames, L.L. and Sand, L.B. (1958) Factors effecting maximum hydrothermal stability in montmorillonites. *American Mineralogist*, **43**, 641–648.
- Archer, P.D.J., Franz, H.B., Sutter, B., Arevalo, R.D.J., Coll, P., Eigenbrode, J.L., Glavin, D.P., Jones, J.J., Leshin, L.A., Mahaffy, P.R., McAdam, A.C., McKay, C.P., Ming, D.W., Morris, R. V., Navarro-González, R., Niles, P.B., Pavlov, A., Squyres, S.W., Stern, J.C., Steele, A., and Wray, J.J. (2014) Abundances and implications of volatile-bearing species from evolved gas analysis of the Rocknest aeolian deposit, Gale Crater, Mars. *Journal of Geophysical Research: Planets*, **119**, 237–254.
- Arvidson, R.E., Squyres, S.W., Bell, J.F., Catalano, J.G., Clark, B.C., Crumpler, L.S., de Souza, P.A., Fairén, A.G., Farrand, W.H., Fox, V.K., Gellert, R., Ghosh, A., Golombek, M.P., Grotzinger, J.P., Guinness, E.A., Herkenhoff, K.E., Jolliff, B.L., Knoll, A.H., Li, R., McLennan, S.M., Ming, D.W., Mittlefehldt, D.W., Moore, J.M., Morris, R.V., Murchie, S.L., Parker, T.J., Paulsen, G., Rice, J.W., Ruff, S.W., Smith, M.D., and Wolff, M.J. (2014) Ancient aqueous environments at Endeavour crater, Mars. *Science*, **343**, doi: 10.1126/science.1248097.
- Bibring, J., Langevin, Y., Gendrin, A., Gondet, B., Poulet, F., Berthé, M., Soufflot, A., Arvidson, R., Mangold, N., Mustard, J., Drossart, P., and OMEGA Team (2005) Mars surface diversity as revealed by the OMEGA/Mars Express observations. *Science*, **307**, 1576–1581.
- Bibring, J., Langevin, Y., Mustard, J., Poulet, F., Arvidson, R., Gendrin, A., Gondet, B., Mangold, N., Pinet, P., Forget, F., and OMEGA Team (2006) Global mineralogical and aqueous Mars history derived from OMEGA/Mars Express data. *Science*, **312**, 400–404.
- Bischoff, A. and Stöfler, D. (1992) Shock metamorphism as a



- fundamental process in the evolution of planetary bodies: Information from meteorites. *European Journal of Mineralogy*, **4**, 707–755.
- Bishop, J.L., Pieters, C.M., and Edwards, J.O. (1994) Infrared spectroscopic analyses on the nature of water in montmorillonite. *Clays and Clay Minerals*, **42**, 702–716.
- Bishop, J., Murad, E., and Dyar, M.D. (2002a) The influence of octahedral and tetrahedral cation substitution on the structure of smectites and serpentines as observed through infrared spectroscopy. *Clay Minerals*, **37**, 617–628.
- Bishop, J., Madejová, J., Komadel, P., and Fröschl, H. (2002b) The influence of structural Fe, Al and Mg on the infrared OH bands in spectra of dioctahedral smectites. *Clay Minerals*, **37**, 607–616.
- Bishop, J.L., Noe Dobra, E.Z., McKeown, N.K., Parente, M., Ehlmann, B.L., Michalski, J.R., Milliken, R.E., Poulet, F., Swayze, G.A., Mustard, J.F., Murchie, S.L., and Bibring, J.-P. (2008a) Phyllosilicate diversity and past aqueous activity revealed at Mawrth Vallis, Mars. *Science*, **321**, 830–833.
- Bishop, J., Lane, M., Dyar, M., and Brown, A. (2008b) Reflectance and emission spectroscopy study of four groups of phyllosilicates: smectites, kaolinite-serpentines, chlorites and micas. *Clay Minerals*, **43**, 35–54.
- Bogard, D.D. and Hirsch, W.C. (1980)  $^{40}\text{Ar}/^{39}\text{Ar}$  dating, Ar diffusion properties, and cooling rate determinations of severely shocked chondrites. *Geochimica et Cosmochimica Acta*, **44**, 1667–1682.
- Boslough, M.B., Weldon, R.J., and Ahrens, T.J. (1980) Impact-induced water loss from serpentine, nontronite and kernite. Pp. 2145–2158 in *Proceedings of the Eleventh Lunar and Planetary Science Conference*, Houston, Texas, USA, March 17–21, 1980 (R.B. Merrill, editor) *Geochimica et Cosmochimica Acta*, Supplement **11**, Pergamon Press, Inc., New York, New York.
- Boslough, M., Venturini, E., Morosin, B., Graham, R., and Williamson, D. (1986) Physical properties of shocked and thermally altered nontronite: Implications for the Martian surface. *Journal of Geophysical Research*, **91**, E207–E214.
- Boslough, M.B., Cygan, R.T., and Izett, G.A. (1995) NMR spectroscopy of quartz from the K/T Boundary: Shock-induced peak broadening, dense glass, and coesite. *Twenty-sixth Lunar and Planetary Science Conference*, Lunar and Planetary Institute Contribution 1592, Abstract #1075
- Brearley, A.J. (2000) Hydrous phases in ALH84001: Further evidence for preterrestrial alteration and a shock-induced thermal overprint. *Thirty-first Lunar and Planetary Science Conference*, Lunar and Planetary Institute Contribution 1000, Abstract #1203.
- Carroll, D.L., Kemp, T.F., Bastow, T.J., and Smith, M.E. (2005) Solid-state NMR characterisation of the thermal transformation of a Hungarian white illite. *Solid State Nuclear Magnetic Resonance*, **28**, 31–43.
- Carter, J., Poulet, F., Bibring, J.-P., Mangold, N., and Murchie, S. (2013) Hydrous minerals on Mars as seen by the CRISM and OMEGA imaging spectrometers: Updated global view. *Journal of Geophysical Research: Planets*, **118**, 831–858.
- Chao, E.C.T., Fahey, J.J., and Littler, J. (1962) Stishovite,  $\text{SiO}_2$ , a very high pressure new mineral from Meteor Crater, Arizona (Late Letter to the Editor). *Journal of Geophysical Research*, **67**(1), 419–421.
- Che, C. and Glotch, T.D. (2012) The effect of high temperatures on the mid-to-far-infrared emission and near-infrared reflectance spectra of phyllosilicates and natural zeolites: Implications for martian exploration. *Icarus*, **218**, 585–601.
- Che, C. and Glotch, T.D. (2014) Thermal alteration: A possible reason for the inconsistency between OMEGA/CRISM and TES detections of phyllosilicates on Mars? *Geophysical Research Letters*, **41**, 321–327.
- Che, C., Glotch, T., Bish, D., Michalski, J.R., and Xu, W. (2011) Spectroscopic study of the dehydration and/or dehydroxylation of phyllosilicate and zeolite minerals. *Journal of Geophysical Research*, **116**, E05007, doi: 10.1029/2010JE003740.
- Cheetham, A.K., Clayden, N.J., Dobson, C.M., and Jakeman, R.J.B. (1986) Correlations between  $^{31}\text{P}$  n.m.r. chemical shifts and structural parameters in crystalline inorganic phosphates. *Journal of the Chemical Society, Chemical Communications*, **3**, 195–197.
- Clark, B.C., Arvidson, R.E., Gellert, R., Morris, R.V., Ming, D.W., Richter, L., Ruff, S.W., Michalski, J.R., Farrand, W.H., Yen, A., Herkenhoff, K.E., Li, R., Squyres, S.W., Schröder, C., Klingelhöfer, G., and Bell, J.F. (2007) Evidence for montmorillonite or its compositional equivalent in Columbia Hills, Mars. *Journal of Geophysical Research*, **112**, E06S01, doi: 10.1029/2006JE002756.
- Clark, R.N. (1999) Chapter 1: Spectroscopy of rocks and minerals, and principles of spectroscopy. Pp. 3–58 in: *Manual of Remote Sensing, Volume 3, Remote Sensing for the Earth Sciences* (A.N. Rencz, editor). John Wiley and Sons, New York, USA.
- Cygan, R.T., Boslough, M.B., and Kirkpatrick, R.J. (1992) NMR spectroscopy of experimentally shocked quartz and plagioclase feldspar powders. Pp. 127–136 in *Proceedings of the Twenty-second Lunar and Planetary Science Conference*, Houston, Texas, USA, March 18–22, 1991 (G. Ryder and V.L. Sharpton, editors). Lunar and Planetary Institute, Houston, Texas, USA.
- d’Espinoze de Lacaille, J.-B., Fretigny, C., and Massiot, D. (2008) MAS NMR spectra of quadrupolar nuclei in disordered solids: The Czjzek model. *Journal of Magnetic Resonance*, **192**, 244–251.
- Daly, T., Gavin, P., and Chevrier, V. (2011) Effects of thermal alteration on the near-infrared and mid-infrared spectra of martian phyllosilicates. *Forty-second Lunar and Planetary Science Conference*, Lunar and Planetary Institute Contribution 1608, Abstract #1164.
- De Carli, P.S. and Jamieson, J.C. (1959) Formation of an amorphous form of quartz under shock conditions. *The Journal of Chemical Physics*, **31**, 1675–1676.
- Delineau, T., Allard, T., Muller, J.P., Barres O., Yvon, J., and Cases, J.M. (1994) FTIR reflectance vs. EPR studies of structural iron in kaolinites. *Clays and Clay Minerals*, **42**, 308–320.
- Eberl, D., Whitney, G., and Khoury, H. (1978) Hydrothermal reactivity of smectite. *American Mineralogist*, **63**, 401–409.
- Ehlmann, B.L., Mustard, J.F., Swayze, G. A., Clark, R.N., Bishop, J.L., Poulet, F., Des Marais, D.J., Roach, L.H., Milliken, R.E., Wray, J.J., Barnouin-Jha, O., and Murchie, S.L. (2009) Identification of hydrated silicate minerals on Mars using MRO-CRISM: Geologic context near Nili Fossae and implications for aqueous alteration. *Journal of Geophysical Research*, **114**, E00D08, doi: 10.1029/2009JE003339.
- Ehlmann, B.L., Mustard, J.F., Murchie, S.L., Bibring, J.-P., Meunier, A., Fraeman, A.A., and Langevin, Y. (2011) Subsurface water and clay mineral formation during the early history of Mars. *Nature*, **479** (7371), 53–60.
- Ehlmann, B.L., Bish, D.L., Ruff, S.W., Mustard, J.F. (2012) Mineralogy and chemistry of altered Icelandic basalts: Application to clay mineral detection and understanding aqueous environments on Mars. *Journal of Geophysical Research*, **117**, E00J16, doi: 10.1029/2012JE004156.
- Ehlmann, B.L., Berger, G., Mangold, N., Michalski, J.R., Catling, D.C., Ruff, S.W., Chassefière, E., Niles, P.B., Chevrier, V., and Poulet, F. (2013) Geochemical consequences of widespread clay mineral formation in Mars’ ancient crust. *Space Science Reviews*, **174**, 329–364.

- Engelhardt, G. and Michel, D. (1987) *High-resolution Solid-State NMR of Silicates and Zeolites*. John Wiley and Sons, New York, 499 pp.
- Fahrenfort, J. (1961) Attenuated total reflection: A new principle for the production of useful infra-red reflection spectra of organic compounds. *Spectrochimica Acta*, **17**, 698–709.
- Fairén, A.G., Chevrier, V., Abramov, O., Marzo, G.A., Gavin, P., Davila, A.F., Tornabene, L.L., Bishop, J.L., Roush, T.L., Gross, C., Kneissl, T., Uceda, E.R., Dohm, J.M., Schulze-Makuch, D., Rodríguez, J.A.P., Amils, R., and McKay, C.P. (2010) Noachian and more recent phyllosilicates in impact craters on Mars. *Proceedings of the National Academy of Sciences of the United States of America*, **107**, 12095–12100.
- Farmer, V.C. (1968) Infrared spectroscopy in clay mineral studies. *Clay Minerals*, **7**, 373–387.
- Fiske, P.S., Nellis, W.J., Xu, Z., and Stebbins, J.F. (1998) Shocked quartz: A  $^{29}\text{Si}$  magic-angle-spinning nuclear magnetic resonance study. *American Mineralogist*, **83**, 1285–1292.
- Fitzgerald, J.J., Hamza, A.I., Dec, S.F., and Bronnimann, C.E. (1996) Solid-state  $^{27}\text{Al}$  and  $^{29}\text{Si}$  NMR and  $^1\text{H}$  CRAMPS studies of the thermal transformations of the 2:1 phyllosilicate pyrophyllite. *Journal of Physical Chemistry*, **3654**, 17351–17360.
- French, B.M. (1968) Shock metamorphism as a geologic process. Pp. 1–17 in: *Shock Metamorphism of Natural Materials: Proceedings of the First Conference Held at NASA, Goddard Space Flight Center, Greenbelt, Maryland, April 14-16, 1966* (B.M. French and N.M. Short, editors). Mono Book Corp., Baltimore, Maryland, USA.
- French, B.M. (1998) *Traces of Catastrophe: A Handbook of Shock-Metamorphic Effects in Terrestrial Meteorite Impact Structures*. LPI Contribution 954, Lunar and Planetary Institute, Houston, Texas, USA.
- Friedlander, L.R., Glotch, T.D., Bish, D.L., Dyar, M.D., Sharp T.G., Sklute, E.C., and Michalski, J.R. (2015) Structural and spectroscopic changes to natural nontronite induced by experimental impacts between 10 and 40 GPa. *Journal of Geophysical Research: Planets*, **120**, 888–912.
- Furukawa, Y., Sekine, T., Kakegawa, T., and Nakazawa, H. (2011) Impact-induced phyllosilicate formation from olivine and water. *Geochimica et Cosmochimica Acta*, **75**, 6461–6472.
- Gault, D.E. and Heitowitz, E.D. (1963) The partition of energy for hypervelocity impact craters formed in rock. Pp. 1–38 in: *Proceedings of the 6th Hypervelocity Impact Symposium*. National Aeronautics and Space Administration, Cleveland, Ohio/Moffett Field, California.
- Gavin, P. and Chevrier, V. (2010) Thermal alteration of nontronite and montmorillonite: Implications for the martian surface. *Icarus*, **208**, 721–734.
- Gavin, P., Chevrier, V., Ninagawa, K., Gucsik, A., and Hasagawa, S. (2013) Experimental investigation into the effects of meteoritic impacts on the spectral properties of phyllosilicates on Mars. *Journal of Geophysical Research: Planets*, **118**, 1–16.
- Gibbons, R. V. and Ahrens, T.J. (1971) Shock metamorphism of silicate glasses. *Journal of Geophysical Research*, **76**, 5489–5498.
- Glotch, T.D., Rossman, G.R., and Aharonson, O. (2007) Mid-infrared (5–100  $\mu\text{m}$ ) reflectance spectra and optical constants of ten phyllosilicate minerals. *Icarus*, **192**, 605–622.
- Gooding, J.L., Aggrey, K.E., and Muenow, D.W. (1990) Volatile compounds in shergottite and nakhlite meteorites. *Meteoritics and Planetary Science*, **25**, 281–289.
- Gooding, J.L., Wentworth, S.J., and Zolensky, M.E. (1991) Aqueous alteration of the Nakhla meteorite. *Meteoritics and Planetary Science*, **26**, 135–143.
- Grieve, R.A.F., Langenhorst, F., and Stöffler, D. (1996) Invited Review: Shock metamorphism of quartz in nature and experiment: II. Significance in geoscience. *Meteoritics and Planetary Science*, **31**, 6–35.
- Grotzinger, J.P., Sumner, D.Y., Kah, L.C., Stack, K., Gupta, S., Edgar, L., Rubin, D., Lewis, K., Schieber, J., Mangold, N., Milliken, R., Conrad, P.G., DesMarais, D., Farmer, J., Siebach, K., Calef, F., Hurowitz, J., McLennan, S.M., Ming, D., Vaniman, D., Crisp, J., Vasavada, A., Edgett, K.S., Malin, M., Blake, D., Gellert, R., Mahaffy, P., Wiens, R.C., Maurice, S., Grant, J.A., Wilson, S., Anderson, R.C., Beegle, L., Arvidson, R., Hallet, B., Sletten, R.S., Rice, M., Bell, J., Griffes, J., Ehlmann, B., Anderson, R.B., Bristow, T.F., Dietrich, W.E., Dromart, G., Eigenbrode, J., Fraeman, A., Hardgrove, C., Herkenhoff, K., Jandura, L., Kocurek, G., Lee, S., Leshin, L.A., Leveille, R., Limonadi, D., Maki, J., McCloskey, S., Meyer, M., Miniti, M., Newsom, H., Oehler, D., Okon, A., Palucis, M., Parker, T., Rowland, S., Schmidt, M., Squyres, S., Steele, A., Stolper, E., Summons, R., Treiman, A., Williams, R., and Yingst, A. (2014) A habitable fluvio-lacustrine environment at Yellowknife Bay, Gale Crater, Mars. *Science*, **343**, doi: 10.1126/science.1242777.
- Hamilton, V.E., Christensen, P.R., McSween, H.Y. Jr., Bandfield, J.L. (2003) Searching for the source regions of martian meteorites using MGS TES: Integrating martian meteorites into the global distribution of igneous materials on Mars. *Meteoritics and Planetary Science*, **38**, 871–885.
- Hanss, R.E., Montague, M.K., Davis, C., and Galindo, C. (1978) X-ray diffractometer studies of shocked materials. Pp. 2773–2787 in: *Proceedings of the Ninth Lunar and Planetary Science Conference*, Houston, Texas, USA, March 13-17, 1978, Volume 2 (R.B. Merrill, editor). *Geochimica et Cosmochimica Acta*, Supplement **9**, Pergamon Press, Inc., New York, New York, USA.
- Harris, W.G., Hollien, K.A., Bates, S.R., and Acree, W.A. (1992) Dehydration of hydroxy-interlayered vermiculite as a function of time and temperature. *Clays and Clay Minerals*, **40**, 335–340.
- Hartmann, W.K. (1966) Martian cratering. *Icarus*, **5**, 565–576.
- Hartmann, W.K. and Neukum, G. (2001) Cratering chronology and the evolution of Mars. *Space Science Reviews*, **96**, 165–194.
- Hayashi, S. and Hayamizu, K. (1990) Accurate determination of NMR chemical shifts in alkali halides and their correlation with structural factors. *Bulletin of the Chemical Society of Japan*, **63**, 913–919.
- Hayashi, S., Ueda, T., Hayamizu, K., and Akiba E. (1992) NMR study of kaolinite. 1.  $^{29}\text{Si}$ ,  $^{27}\text{Al}$  and  $^1\text{H}$  spectra. *Journal of Physical Chemistry* **96**, 10922–10928.
- Hörz, F. and Ahrens, T.J. (1969) Deformation of experimental shocked biotite. *American Journal of Science*, **267**, 1213–1229.
- Hugoniot, H. (1889) Sur la propagation du mouvement dans les corps et spécialement dans les gaz parfaits. *Journal de l'École Polytechnique*, **58**, 1–125.
- Johnson, J., Hörz, F., Lucey, P.G., and Christensen, P.R. (2002) Thermal infrared spectroscopy of experimentally shocked anorthosite and pyroxenite: Implications for remote sensing of Mars. *Journal of Geophysical Research*, **107**, 5073.
- Johnson, J.R. and Hörz, F. (2003) Visible/near-infrared spectra of experimentally shocked plagioclase feldspars. *Journal of Geophysical Research*, **108**, 5120.
- Johnson, J.R., Staid, M.I., and Kraft, M.D. (2007) Thermal infrared spectroscopy and modeling of experimentally shocked basalts. *American Mineralogist*, **92**, 1148–1157.
- Kieffer, S.W. (1971) Shock metamorphism of the Coconino

- Sandstone at Meteor Crater, Arizona. *Journal of Geophysical Research*, **76**, 5449–5473.
- Kieffer, S.W., Schaal, R.B., Gibbons, R., Hörz, F., Milton, D.J., and Dube, A. (1976) Shocked basalt from Lonar Impact Crater, India and experimental analogues. Pp. 1391–1412 in: *Proceedings of the Seventh Lunar and Planetary Science Conference*, Houston, Texas, USA, March 15–19, 1976, Volume 2 (R.B. Merrill, Editor). *Geochimica et Cosmochimica Acta*, Supplement 7, New York, New York, Pergamon Press, Inc..
- Kloppogge, J. and Frost, R. (2001) Infrared emission spectroscopic study of the dehydroxylation of some natural and synthetic saponites. *Neues Jahrbuch für Mineralogie Abhandlungen*, **Jg. 2001**, 446–463.
- Kraus, R.G., Stewart, S.T., Newman, M.G., Milliken, R.E., and Tosca, N.J. (2013) Uncertainties in the shock devolatilization of hydrated minerals: A nontronite case study. *Journal of Geophysical Research: Planets*, **118**, 2137–2145.
- Kulbicki, G. (1959) High temperature phases in sepiolite, attapulgite and saponite. *American Mineralogist*, **44**, 752–764.
- Lange, M.A. and Ahrens, T.J. (1982) Impact induced dehydration of serpentine and the evolution of planetary atmospheres. *Journal of Geophysical Research*, **87**, A451–A456.
- Langenhorst, F. (2002) Shock metamorphism of some minerals: Basic introduction and microstructural observations. *Bulletin of the Czech Geological Survey*, **77**, 265–282.
- Laperche, V., Lambert, J.F., Prost, R., and Fripiat, J.J. (1990) High-resolution solid-state NMR of exchangeable cations in the interlayer surface of a swelling mica:  $^{23}\text{Na}$ ,  $^{111}\text{Cd}$ , and  $^{133}\text{Cs}$  vermiculites. *Journal of Physical Chemistry*, **94**, 8821–8831.
- Lipsicas, M., Raythatha, R.H., Pinnavaia, T.J., Johnson, I.D., Giese, R.F., Costanzo, P.M., and Robert, J.L. (1984) Silicon and aluminum site distributions in 2:1 layered silicate clays. *Nature*, **309**, 604–607.
- Loizeau, D., Mangold, N., Poulet, F., Bibring, J., Gendrin, A., Ansan, V., Gomez, C., Gondet, B., Langevin, Y., Masson, P., and Neukum, G. (2007) Phyllosilicates in the Mawrth Vallis region of Mars. *Journal of Geophysical Research*, **112**, E08S08.
- Madejová, J. and Komadel, P. (2001) Baseline studies of the Clay Minerals Society Source Clays: Infrared methods. *Clays and Clay Minerals*, **49**, 410–432.
- Magi, M., Lippmaa, E., Samoson, A., Engelhardt, G., and Grimmer, A.R. (1984) Solid-state high-resolution silicon-29 chemical shifts in silicates. *Journal of Physical Chemistry*, **88**, 1518–1522.
- Mangold, N., Poulet, F., Mustard, J., Bibring, J., Gondet, B., Langevin, Y., Ansan, V., Masson, P., Fassett, C., Head, J., Hoffmann, H., and Neukum, G. (2007) Mineralogy of the Nili Fossae region with OMEGA/Mars Express data: 2. Aqueous alteration of the crust. *Journal of Geophysical Research*, **112**, E08S04.
- Marzo, G.A., Davila, A.F., Tornabene, L.L., Dohm, J.M., Fairén, A.G., Gross, C., Kneissl, T., Bishop, J.L., Roush, T.L., and McKay, C.P. (2010) Evidence for Hesperian impact-induced hydrothermalism on Mars. *Icarus*, **208**, 667–683.
- Massiot, D., Dion, P., Alcover, J.F., and Bergaya, F. (1995)  $^{27}\text{Al}$  and  $^{29}\text{Si}$  MAS NMR study of kaolinite thermal decomposition by controlled rate thermal analysis. *Journal of the American Ceramic Society*, **78**, 2940–2944.
- McKeown, N., Bishop, J., Noe Dobrea, E., Ehlmann, B., Parente, M., Mustard, J., Murchie, S., Swayze, G., Bibring, J., and Silver, E. (2009) Characterization of phyllosilicates observed in the central Mawrth Vallis region, Mars, their potential formational processes, and implications for past climate. *Journal of Geophysical Research*, **114**, E00D10.
- McSween, H.Y. Jr. (1994) What we have learned about Mars from SNC meteorites. *Meteoritics*, **29**, 757–779.
- Meinhold, R.H., Atakul, H., Davies, T.W., and Slade, R.C.T. (1992) Flash calcines of kaolinite: Kinetics of isothermal dehydroxylation of partially dehydroxylated flash calcines and of flash calcination itself. *Journal of Materials Chemistry*, **2**, 913–921.
- Meinhold, R.H., Slade, R.C.T., and Davies, T.W. (1993) High-field  $^{27}\text{Al}$  MAS NMR studies of the formation of metakaolinite by flash calcination of kaolinite. *Applied Magnetic Resonance*, **4**, 141–155.
- Mermut, A.R. and Cano, A.F. (2001) Baseline studies of the Clay Minerals Society Source Clays: Chemical analyses of major elements. *Clays and Clay Minerals*, **49**, 381–386.
- Michalski, J.R. and Noe Dobrea, E.Z. (2007) Evidence for a sedimentary origin of clay minerals in the Mawrth Vallis region, Mars. *Geology*, **35**, 951–954.
- Michalski, J.R., Kraft, M.D., Sharp, T.G., Williams, L.B., and Christensen, P.R. (2005) Mineralogical constraints on the high-silica martian surface component observed by TES. *Icarus*, **174**, 161–177.
- Michalski, J.R., Kraft, M.D., Sharp, T.G., Williams, L.B., and Christensen, P.R. (2006) Emission spectroscopy of clay minerals and evidence for poorly crystalline aluminosilicates on Mars from Thermal Emission Spectrometer data. *Journal of Geophysical Research*, **111**, E03004, doi: 10.1029/2005JE002438.
- Michalski, J., Poulet, F., Bibring, J.-P., and Mangold, N. (2010) Analysis of phyllosilicate deposits in the Nili Fossae region of Mars: Comparison of TES and OMEGA data. *Icarus*, **206**, 269–289.
- Moll, W.F. Jr. (2001) Baseline studies of the Clay Minerals Society Source Clays: Geological origin. *Clays and Clay Minerals*, **49**, 374–380.
- Moore, D.M. and Reynolds, R.C.J. (1989) *X-Ray Diffraction and the Identification and Analysis of Clay Minerals*. Oxford University Press, Oxford UK. 332 pp.
- Moskowitz, B.M. and Hargraves, R.B. (1984) Magnetic cristobalite (?): A possible new magnetic phase produced by the thermal decomposition of nontronite. *Science*, **255**, 1152–1154.
- Murchie, S.L., Mustard, J.F., Ehlmann, B.L., Milliken, R.E., Bishop, J.L., McKeown, N.K., Noe Dobrea, E.Z., Seelos, F.P., Buczkowski, D.L., Wiseman, S.M., Arvidson, R.E., Wray, J.J., Swayze, G., Clark, R.N., Des Marais, D.J., McEwen, A.S., and Bibring, J.-P. (2009) A synthesis of Martian aqueous mineralogy after 1 Mars year of observations from the Mars Reconnaissance Orbiter. *Journal of Geophysical Research*, **114**, E00D06, doi: 10.1029/2009JE003342.
- Mustard, J.F., Murchie, S.L., Pelkey, S.M., Ehlmann, B.L., Milliken, R.E., Grant, J.A., Bibring, J.-P., Poulet, F., Bishop, J., Noe Dobrea, E., Roach, L., Seelos, F., Arvidson, R.E., Wiseman, S., Green, R., Hash, C., Humm, D., Malaret, E., McGovern, J.A., Seelos, K., Clancy, T., Clark, R., Des Marais, D., Izenberg, N., Knudson, A., Langevin, Y., Martin, T., McGuire, P., Morris, R., Robinson, M., Roush, T., Smith, M., Swayze, G., Taylor, H., Titus, T., and Wolff, M. (2008) Hydrated silicate minerals on Mars observed by the Mars Reconnaissance Orbiter CRISM instrument. *Nature*, **454**, 305–309.
- Mustard, J.F., Ehlmann, B.L., Murchie, S.L., Poulet, F., Mangold, N., Head, J.W., Bibring, J.-P., and Roach, L.H. (2009) Composition, morphology, and stratigraphy of Noachian crust around the Isidis basin. *Journal of Geophysical Research*, **114**, E00D12, doi: 10.1029/2009JE003349.
- Newman, R.H., Childs, C.W., and Churchman, G.J. (1994) Aluminum coordination and structural disorder in halloysite

- and kaolinite by  $^{27}\text{Al}$  NMR spectroscopy. *Clay Minerals*, **29**, 305–312.
- Petit, S., Madejová, J., Decarreau, A., and Martin, F. (1999) Characterization of octahedral substitutions in kaolinites using near infrared spectroscopy. *Clays and Clay Minerals*, **47**, 103–108.
- Petit, S., Decarreau, A., Martin, F., and Buchet, R. (2004) Refined relationship between the position of the fundamental OH stretching and the first overtones for clays. *Physics and Chemistry of Minerals*, **31**, 585–592.
- Post, J.L. (1984) Saponite from near Ballarat, California. *Clays and Clay Minerals*, **32**, 147–153.
- Poulet, F., Bibring, J., Mustard, J., Gendrin, A., Mangold, N., Langevin, Y., Arvidson, R., Gondet, B., Gomez, C., Berthé, M., Erard, S., Forni, O., Manaud, N., Poulleau, G., Soufflot, A., Combes, M., Drossart, P., Encrenaz, T., Fouchet, T., Melchiorri, R., Bellucci, G., Altieri, F., Formisano, V., Fonti, S., Capaccioni, F., Ceroni, P., Coradini, A., Korablev, O., Kottsov, V., Ignatiev, N., Titov, D., Zasova, L., Pinet, P., Schmitt, B., Sotin, C., Hauber, E., Hoffmann, H., Jaumann, R., Keller, U., and Forget, F. (2005) Phyllosilicates on Mars and implications for early martian climate. *Nature*, **438**, 623–627.
- Poulet, F., Mangold, N., Loizeau, D., Bibring, J., Langevin, Y., Michalski, J., and Gondet, B. (2008) Abundance of minerals in the phyllosilicate-rich units on Mars. *Astronomy and Astrophysics*, **487**, L41–L44.
- Poulet, F., Beaty, D., Bibring, J., Bish, D., Bishop, J., Noe Dobra, E., Mustard, J., Petit, S., and Roach, L. (2009) Key scientific questions and key investigations from the First International Conference on Martian Phyllosilicates. *Astrobiology*, **9**, 257–267.
- Pruett, R.J. and Webb, H.L. (1993) Sampling and analysis of KGa-1B well-crystallized kaolin Source Clay. *Clays and Clay Minerals*, **41**, 514–519.
- Rankine, W.J.M. (1870) On the thermodynamic theory of waves of finite longitudinal disturbance. *Proceedings of the Royal Society of London*, **18**, 80–83.
- Roch, G.E., Smith, M.E., and Drachman, S.R. (1998) Solid state NMR characterization of the thermal transformation of an illite-rich clay. *Clays and Clay Minerals*, **46**, 694–704.
- Rocha, J. (1999) Single- and triple-quantum  $^{27}\text{Al}$  MAS NMR study of the thermal transformation of kaolinite. *Journal of Physical Chemistry B*, **103**, 9801–9804.
- Rocha, J. and Klinowski, J. (1990a)  $^{29}\text{Si}$  and  $^{27}\text{Al}$  magic-angle-spinning NMR studies of the thermal transformation of kaolinite. *Physics and Chemistry of Minerals*, **17**, 179–186.
- Rocha, J. and Klinowski, J. (1990b) Solid-state NMR studies of the structure and reactivity of metakaolinite. *Angewandte Chemie International Edition in English*, **29**, 553–554.
- Ruff, S.W., Christensen, P.R., Barbera, P.W., and Anderson, D.L. (1997) Quantitative thermal emission spectroscopy of minerals: A laboratory technique for measurement and calibration. *Journal of Geophysical Research*, **102**, 14,899–14,913.
- Sand, L.B. and Ames, L.L. (1957) Stability and decomposition products of hectorite. *Clays and Clay Minerals*, **6**, 392–398.
- Sanz, J., Sobrados, I., and Robert, J.L. (2015) Influence of hydration on  $^{23}\text{Na}$ ,  $^{27}\text{Al}$ , and  $^{29}\text{Si}$  MAS-NMR spectra of sodium saponites and sodium micas. *American Mineralogist*, **100**, 1076–1083.
- See, T.H., Cardenas, F., and Montes, R. (2012) The Johnson Space Center Experimental Impact Lab: Contributions toward understanding the evolution of the solar system. *Forty-third Lunar and Planetary Science Conference*, Lunar and Planetary Institute Contribution 1659, Abstract #2488.
- Slade, R.C.T. and Davies, T.W. (1991) Evolution of structural changes during flash calcination of kaolinite: A  $^{29}\text{Si}$  and  $^{27}\text{Al}$  nuclear magnetic resonance spectroscopy study. *Journal of Materials Chemistry*, **1**, 361–364.
- Slade, R.C.T., Davies, T.W., and Atakul, H. (1991) Flash calcination of kaolinite: Mechanistic information from thermogravimetry. *Journal of Materials Chemistry*, **1**, 751–756.
- Smith, M.E. (1993) Application of  $^{27}\text{Al}$  NMR techniques to structure determination in solids. *Applied Magnetic Resonance*, **4**, 1–64.
- Stöffler, D. (1972) Deformation and transformation of rock-forming minerals by natural and experimental shock processes: I. Behavior of minerals under shock compression. *Fortschritte der Mineralogie*, **49**, 50–113.
- Stöffler, D. (1974) Deformation and transformation of rock-forming minerals by natural and experimental shock processes: II. Physical properties of shocked minerals. *Fortschritte der Mineralogie*, **51**, 256–289.
- Stöffler, D. (1984) Glasses formed by hypervelocity impact. *Journal of Non-Crystalline Solids*, **67**, 465–502.
- Stöffler, D. and Langenhorst, F. (1994) Shock metamorphism of quartz in nature and experiment: I. Basic observation and theory. *Meteoritics*, **29**, 155–181.
- Tanaka, K.L. (1987) The stratigraphy of Mars. *Proceedings of the Seventeenth Lunar and Planetary Science Conference*, Houston, Texas, USA, March 17–21, 1986 (G. Ryder and G. Schubert, editors) (Part I). *Journal of Geophysical Research*, **91**, E139–E158.
- Tanaka, K.L. (2005) Geology and insolation-driven climatic history of Amazonian north polar materials on Mars. *Nature*, **437**, 991–994.
- Tarte, P., Rulmont, A., Liégeois-Duyckaerts, M., Cahay, R., and Winand, J.M. (1990) Vibrational spectroscopy and solid state chemistry. *Solid State Ionics*, **42**, 177–196.
- Thomas-Keperta, K.L., Wentworth, S.J., Mckay, D.S., and Gibson, E.K. (2000) Field emission gun scanning electron (FEGSEM) and transmission electron (TEM) microscopy of phyllosilicates in martian meteorites ALH84001, Nakhla, and Shergotty. *Thirty-first Lunar and Planetary Science Conference*, Lunar and Planetary Institute Contribution No. 1000, Abstract #1690.
- Tornabene, L.L., Osinski, G.R., McEwen, A.S., Wray, J.J., Craig, M.A., Sapers, H.M., and Christensen, P.R. (2013) An impact origin for hydrated silicates on Mars: A synthesis. *Journal of Geophysical Research: Planets*, **118**, 994–1012.
- Treiman, A.H., Barrett, R.A., and Gooding, J.L. (1993) Preterrestrial aqueous alteration of the Lafayette (SNC) meteorite. *Meteoritics and Planetary Science*, **28**, 86–97.
- Tyburczy, J.A. and Ahrens, T.J. (1987) Dehydration kinetics of shocked serpentine. Pp. 435–441 in: *Proceedings of the Eighteenth Lunar and Planetary Science Conference*, Houston, Texas, USA, March 16–20, 1987 (G. Ryder, editor). Cambridge and New York/Houston, Texas, USA, Cambridge University Press/Lunar and Planetary Institute.
- Vaniman, D.T., Bish, D.L., Ming, D.W., Bristow, T.F., Morris, R.V., Blake, D.F., Chipera, S.J., Morrison, S.M., Treiman, A.H., Rampe, E.B., Rice, M., Achilles, C.N., Grotzinger, J.P., McLennan, S.M., Williams, J., Bell, J.F., Newsom, H.E., Downs, R.T., Maurice, S., Sarrazin, P., Yen, A.S., Morookian, J.M., Farmer, J.D., Stack, K., Milliken, R.E., Ehlmann, B.L., Sumner, D.Y., Berger, G., Crisp, J.A., Hurowitz, J.A., Anderson, R., Des Marais, D.J., Stolper, E.M., Edgett, K.S., Gupta, S., and Spanovich, N. (2014) Mineralogy of a mudstone at Yellowknife Bay, Gale crater, Mars. *Science*, **343**, doi: 10.1126/science.1243480.
- Weiss, C.A., Altaner, S.P., and Kirkpatrick, R.J. (1987) High-resolution  $^{29}\text{Si}$  NMR spectroscopy of 2:1 layer silicates: Correlations among chemical shift, structural distortions, and chemical variations. *American Mineralogist*, **72**, 935–942.
- Weldon, R.J., Thomas, W.M., Boslough, M.B., and Ahrens,

- T.J. (1982) Shock-induced color changes in nontronite: Implications for the martian fines. *Journal of Geophysical Research*, **87**, 10,102–10,114.
- Wiseman, S.M., Arvidson, R.E., Morris, R. V., Poulet, F., Andrews-Hanna, J.C., Bishop, J.L., Murchie, S.L., Seelos, F.P., Des Marais, D., and Griffes, J.L. (2010) Spectral and stratigraphic mapping of hydrated sulfate and phyllosilicate-bearing deposits in northern Sinus Meridiani, Mars. *Journal of Geophysical Research*, **115**, E00D18, doi: 10.1029/2009JE003354.
- Woessner, D.E. (1989) Characterization of clay minerals by  $^{27}\text{Al}$  nuclear magnetic resonance spectroscopy. *American Mineralogist*, **74**, 203–215.
- Wray, J., Noe Dobrea, E., Arvidson, R., Wiseman, S., Squyres, S., McEwen, A., Mustard, J., and Murchie, S. (2009) Phyllosilicates and sulfates at Endeavour Crater, Meridiani Planum, Mars. *Geophysical Research Letters*, **36**, L21201, doi: 10.1029/2009GL040734.
- (Received 25 November 2014; revised 4 May 2016; Ms. 933; AE: G.D. Chryssikos)